Submitted to ***Canadian Geotechnical Journal***

Quasi-site-specific prediction for deformation modulus of rock mass

Jianye Ching[1], Kok-Kwang Phoon[2], Yuan-Hsun Ho[3], and Meng-Chia Weng[4]

ABSTRACT

A generic rock mass database consisting of 9 parameters is compiled from 225 studies. The 9 parameters include the deformation modulus, elastic modulus, dynamic modulus, rock quality designation, rock mass rating, Q-system, geological strength index of a rock mass as well as intact-rock Young's modulus and intact-rock uniaxial compressive strength. This generic database, labeled as ROCKMass/9/5876, consists of 5876 rock mass cases. The goal of this paper is to examine how an existing transformation model such as deformation modulus versus rock mass rating can be made more unbiased and more precise for a specific site by combining sparse site data with ROCKMass/9/5876 in a manner sensitive to site-specific differences. The outcome is a quasi-site-specific transformation model. Four methods are studied to construct a quasi-site-specific transformation model for the deformation modulus of a rock mass: probabilistic multiple regression (current state of practice), hybridization method, hierarchical Bayesian model, and similarity method. The results from two case studies in Turkey show that the hierarchical Bayesian model is the most effective.

[1] (Corresponding author) Professor, Dept of Civil Engineering, National Taiwan University, Taiwan. Email: jyching@gmail.com. Tel: +886-2-33664328.
[2] Professor, Dept of Civil and Environmental Engineering, National University of Singapore, Singapore.
[3] Graduate Student, Dept of Civil Engineering, National Taiwan University, Taiwan.
[4] Professor, Dept of Civil Engineering, National Chiao Tung University, Taiwan.

Key words: rock mass properties; ROCKMass/9/5876; deformation modulus; rock mass classification system; quasi-site-specific transformation model; hierarchical Bayesian model.

INTRODUCTION

The deformation modulus (E_m) of an in situ rock mass is a key design parameter. It is not straightforward to determine E_m in the laboratory because E_m is size-dependent. In practice, E_m is commonly determined by an in situ test, such as plate-loading test. Besides the use of in situ tests that are costly, another common method of estimating E_m is through the use of a transformation model (Phoon and Kulhawy 1999a) that predicts E_m based on rock mass parameters, such as rock mass rating (RMR) (Bieniawski 1973). Such transformation models are abundant in the literature (e.g., Zhang 2016, 2017). Transformation models are not exact, and the difference between model prediction and observed value is called transformation uncertainty (Phoon and Kulhawy 1999a).

Most transformation models in the geotechnical literature are generic models (Ching 2018), because they are calibrated by data that are not limited to a single site. A generic model is usually not precise for a specific site. To illustrate this, Figure 1a shows the relationship between RMR and E_m for three sites situated in sedimentary rock: Khersan II dam site, Iran (Ajalloeian and Mohammadi 2014), Neveda site, USA (Keffeler 2014), and Gotvand dam site, Iran (Nejati et al. 2014). Generic transformation models proposed by Bieniawski (1978), Serafim and Pereira (1983), and Gokceoglu et al. (2003) are also plotted. The following observations are obtained: (a) The RMR-E_m trends are strongly site-specific (site uniqueness); (b) a generic transformation model may not fit a site-specific

trend well, and the generic models also differ from one another significantly. To address the problem of site uniqueness, which is a key feature in geotechnical and rock engineering, a site-specific (local) model constructed by site-specific data is more desirable than a generic one. However, site data for many projects are sparse, so a site-specific model cannot be constructed reliably. For instance, Figure 1b shows the RMR-E_m data for a Portugal site, the Miranda hydroelectric project (Sousa et al. 1999). Only four borehole tests (dilatometer) are available to determine E_m. It is not feasible to construct a reliable site-specific model based on the sparse data.

The idea of augmenting sparse site-specific data by a generic database is not new as engineers have been relying on data from similar sites to inform their understanding of a new site. Engineers primarily relies on their experiences and knowledge of local geology to supplement site-specific data with data from other sites judged to be similar in their neighbourhood. There are three limitations. One, experience cannot be readily transferred from one engineer to the next. Second, the practice of a typical engineer is restricted geographically. He/she cannot judge the relevance of a much larger dataset lying outside the domain of local practice. Finally, it is difficult to imagine screening records in a large multivariate database manually. The development of algorithms that can "learn" the unique data features at a specific site and use these features to refine a generic database so that it can supplement sparse site-specific with more relevant data is called the "site challenge" (Phoon 2020).

To address this site challenge for clay sites, Ching and Phoon (2014a), Ching and Phoon (2019, 2020), and Ching et al. (2020) proposed the idea of augmenting sparse site-specific data by a generic clay database (CLAY/10/7490) to construct a quasi-site-specific model. Ching and Phoon (2014a)

proposed a probabilistic multiple regression (PMR) that constructs a generic model based on CLAY/10/7490. The generic model can then be updated by site-specific data into a quasi-site-specific model. Ching and Phoon (2019) proposed a hybridization (HYB) method that constructs a hybrid model by combining a site-specific model with a generic model to produce a quasi-site-specific model. Ching et al. (2020) developed a hierarchical Bayesian model (HBM) that learns the inter-site variability in CLAY/10/7490, and the trained model is then updated using site-specific data to produce a quasi-site-specific model. Ching and Phoon (2020) proposed a method of measuring the similarity (SYM) between a record in CLAY/10/7490 and a site-specific dataset. The records in CLAY/10/7490 with high similarity can be adopted to augment the sparse site-specific data to form a quasi-site-specific dataset.

The problem of site uniqueness in rock engineering is likely to be more pronounced than that in geotechnical engineering (to be elaborated in a later section). To our knowledge, no work has been conducted to understand this site challenge for a rock mass database, which is the focus of this paper. The novelty of this study is two folds:

1. This paper compiles a new generic database for rock mass parameters named ROCKMass/9/5876. This database consists of 5876 rock mass cases from 225 studies for 9 rock mass properties/indices, including rock quality designation (RQD) (Deere 1964), RMR, Q-system (Barton et al. 1974), geological strength index (GSI) (Hoek and Brown 1997), E_m, elastic modulus of rock mass (E_{em}), dynamic modulus of rock mass (E_{dm}), Young's modulus of intact rock (E_i), and uniaxial compressive strength of intact rock (σ_{ci}). The first and second authors have

previously developed an intact rock database ROCK/9/4069 (Ching et al. 2018). Note that ROCKMass/9/5876 and ROCK/9/4069 (Ching et al. 2018) are distinct databases – the former contains rock mass properties; the latter contains intact rock properties. The ROCKMass/9/5876 database contains two intact rock parameters (Young's modulus and uniaxial compressive strength) that are also present in ROCK/9/4069, but only two out of approximately two hundred case studies (references) are common in these databases. Tables 2 to 5 summarize the generic and site-specific statistics for rock mass parameters in ROCKMass/9/5876, whereas Table 6 summarizes the bias and variability of well-known transformation models for the rock mass deformation modulus, E_m. The database ROCKMass/9/5876 as well as the tables are original contributions presented in this paper only.

2. This paper further investigates the four methods (PMR, HYB, HBM, SIM) of constructing a quasi-site-specific E_m transformation model that is supported by ROCKMass/9/5876. These four methods have been mostly adopted to construct quasi-site-specific transformation models for clay properties in the authors' past works. No work has been conducted to construct quasi-site-specific transformation models for rock mass properties. The current study is also the first instance where the four methods are compared in a common rock mass property prediction setting (predicting site-specific E_m). It will be shown that HYB is the most effective while the conventional PMR is the least effective for predicting E_m at a single site.

DATABASE ROCKMASS/9/5876

This study compiles a generic database (ROCKMass/9/5876) from the literature for 9 rock mass parameters. In the literature, generic databases have been compiled for clays, sands, fine-grained soils, and rocks. Table 1 shows some such databases, labelled as (material type)/(number of parameters of interest)/(number of data points). The ROCKMass/9/5876 database consists of 5876 rock mass cases from 225 studies. ROCKMass/9/5876 consists of 17% igneous, 37% sedimentary, and 26% metamorphic cases. The remaining 20% of the cases do not contain rock class information. The geographical regions cover 67 countries/regions in six continents. The parameter values in ROCKMass/9/5876 cover a wide range (RMR from 0 to 97, Q from 0.001 to 1000, GSI from 8 to 100, and E_m from 0.0011 to 104 GPa). The details for ROCKMass/9/5876 are presented in Table S1 in the supplementary material.

The 9 parameters are categorized into three categories:

1. Rock mass index and classifications (RQD, RMR, Q, GSI). There are two versions of RMR, the 1976 version (RMR_{76}) and 1989 version (RMR_{89}). Most RMR data (95%) in ROCKMass/9/5876 are RMR_{89}. The RMR_{76} data are converted to RMR_{89} by $RMR_{89} = RMR_{76} + 5$ (Zhang 2016).
2. Rock mass moduli (E_m, E_{em}, E_{dm}). E_m is the ratio of stress to corresponding total strain during loading of a rock mass, whereas E_{em} is the ratio of stress to corresponding elastic strain. By their definitions, E_m and E_{em} are secant modulus. In ROCKMass/9/5876, 23% of the (E_m, E_{em}) data are measured by plate-bearing tests (plate-loading and plate-jacking tests), 25% by borehole tests (dilatometer and borehole jack tests), 5% by flat jack tests, and 1% by pressure-tunnel tests. The test type is not reported for the remaining 46% of the cases. E_{dm} is calculated from elastic wave

velocity of rock mass.

3. Intact rock properties (E_i and σ_{ci}). In the literature, E_i is reported as a tangent modulus, secant modulus, or average modulus for the linear portion of stress-strain curve. Ching et al. (2018) indicated that the difference between these moduli is less significant in the context of the typical transformation uncertainty associated with E_i correlations (e.g. E_i versus σ_{ci}).

There are 5876 cases in the database. Each "case" is stored as one row in the Excel worksheet that consists of a set of values observed for the same rock mass at approximately the same location and depth. The resulting database is not genuine multivariate in the sense that the 9 parameters are not simultaneously observed, i.e. each row is not completely filled with values. The rightmost column in Table 1 shows the percentage of completeness, defined as (number of filled values)/[(number of parameters)×(number of rows)]. Databases with a value of 100% such as CLAY/5/345 and CLAY/6/535 are genuine multivariate databases. The basic statistics of the 9 parameters are listed in Table 2. The numbers of cases for the 9 rock parameters are shown in the second column of Table 2, in the format of "number of tests (number of data groups)". One "data group" can be broadly interpreted as data from one site or one project. Note that the statistics in Table 2 are not for a specific site but for the entire ROCKMass/9/5876 database. Tables 3 to 5 shows the site-level statistics for the igneous, sedimentary, and metamorphic rock mass. To obtain meaningful second-order site-level statistics, only data groups with no less than 3 data points are considered.

The 9 parameters are denoted by (Y_1, Y_2, …, Y_9):

Y_1 = RQD
Y_2 = RMR

Submitted to ***Canadian Geotechnical Journal***

$$\begin{aligned} Y_3 &= \ln(Q) \\ Y_4 &= GSI \\ Y_5 &= \ln(E_m) \qquad (E_m \text{ in GPa}) \\ Y_6 &= \ln(E_{em}) \qquad (E_{em} \text{ in GPa}) \\ Y_7 &= \ln(E_{dm}) \qquad (E_{dm} \text{ in GPa}) \\ Y_8 &= \ln(E_i) \qquad (E_i \text{ in GPa}) \\ Y_9 &= \ln(\sigma_{ci}) \qquad (\sigma_{ci} \text{ in MPa}) \end{aligned} \tag{1.}$$

The natural logarithm is taken for Q, E_m, E_{em}, E_{dm}, E_i, and σ_{ci} because these parameters cover wide ranges, across more than one order of magnitude. Because the four methods (PMR, HYB, HBM, SIM) operate on the standard normal variables, the Johnson family of distributions (Johnson 1949; Ching and Phoon 2015) is adopted to fit the marginal probability density functions (PDFs) of (Y_1, Y_2, …, Y_9) and subsequently used to convert Y into a standard normal variable X. The fitted results, including the distribution type and the parameters (a_X, b_X, a_Y, b_Y), are summarized in Table S2, and the fitted Johnson PDFs are plotted in Figure S1. The P-values for the Kolmogorov-Smirnov test (Conover 1999) are also shown in the table and figure. With the fitted Johnson marginal PDFs, (Y_1, Y_2, …, Y_9) can be transformed into standard normal variables (X_1, X_2, …, X_9):

$$X = \begin{cases} b_X + a_X \cdot \ln\left[\left(Y - b_Y\right)/a_Y + \sqrt{1 + \left[\left(Y - b_Y\right)/a_Y\right]^2} \right] & \text{Johnson SU} \\ b_X + a_X \cdot \ln\left[\left(Y - b_Y\right)/\left(a_Y + b_Y - Y\right)\right] & \text{Johnson SB} \end{cases} \tag{2.}$$

Correlation trends among (Y_1, Y_2, …, Y_9)

Figure S2 presents the scatter plots between all possible bivariate combinations of (Y_i, Y_j) in ROCKMass/9/5876. The numbers shown in the lower-left of each plot indicate the numbers of cases, in the format of "number of pairwise data (number of data groups)". The trends in Figure S2 are compared with some existing transformation models for rock mass classification. Figure 2 shows the comparison results for the following rock-mass-classification transformation models:

Submitted to ***Canadian Geotechnical Journal***

$$\begin{aligned} &RMR = 9\cdot\ln(Q)+49 && \text{Bieniawski (1976)}\\ &RMR = 15\cdot\ln(Q)+50 && \text{Barton (1995)}\\ &GSI = RMR - 5 && \text{Hoek and Brown (1997)}\\ &GSI = 9\cdot\ln(Q)+44 && \text{Zhang (2016)} \end{aligned} \tag{3.}$$

The original equation proposed by Bieniawski (1976) was $RMR_{76} = 9\ln(Q)+44$. However, the RMR adopted in ROCKMass/9/5876 is RMR_{89}. Because $RMR_{89} \approx RMR_{76}+5$ (Hoek and Brown 1997), this model is revised into $RMR_{89} = 9\ln(Q)+49$, which identifies with the first formula in Eq. (3.). The cases in ROCKMass/9/5876 are annotated by rock class.

The trends in Figure S2 are also compared with some existing E_m transformation models shown in Table 6. The 3rd column in the table shows the application range of each model, which is the range of the calibration dataset for each model. Figure 3 shows the comparison results. For Figures 3b-3d, the vertical axis is presented in a logarithmic scale to allow small values of E_m to be seen. The GSI-E_m models proposed by Beiki et al. (2010) and Hoek and Brown (1997) are not plotted in Figure 3d because their fit to ROCKMass/9/5876 is worse than that for the Hoek-Diederichs model.

The following observations are obtained from Figures 2-3:

1. The ROCKMass/9/5876 "data cloud" covers most transformation models, indicating that ROCKMass/9/5876 has a broad coverage.
2. There is no strong evidence indicating that the correlation trends exhibited by ROCKMass/9/5876 depend on rock class (igneous, sedimentary, and metamorphic). Although not shown, there is no strong evidence indicating that the correlation trends depend on E_m test type (plate-bearing, borehole, flat-jack, and pressure-tunnel tests), either. Note that these observations apply to a generic database covering a broad range of conditions. They do not necessarily apply to one

particular site.

3. In general, data points in ROCKMass/9/5876 exhibit significant scatters around the mean trends, suggesting that the transformation uncertainty is significant. From our experiences, the transformation uncertainty for intact rock or rock mass properties is more significant than that for soil properties. For the RMR-E_m and Q-E_m trends in Figure 3, the data scatter tends to be larger for data points with small E_m.
4. In Figure 2, many rock-mass-classification transformation models in Eq. (3.) fit the generic trends well. In Figure 3, however, many E_m transformation models in Table 6 does not fit the generic trends in well.
5. The transformation models in Eq. (3.) and in Table 6 may not fit a specific site well. For instance, the three RMR-E_m transformation models in Figure 1a do not fit the three sites in the figure well. In general, these models are dataset-specific probably because each model was calibrated by its own dataset. When applying these models to any one specific site outside the database, one must accept the large bias and variability. The bias (b) and COV (δ) for each E_m transformation model in Table 6 are calibrated by ROCKMass/9/5876, where b is the mean ratio of (observed E_m)/(predicted E_m) and δ is the sample COV of this ratio, as defined in Ching and Phoon (2014b) and Ching et al. (2017b, 2018). The resulting b and δ are shown in Table 6: b can be far away from unity, and δ can be large, suggesting that these models can be fairly biased with large transformation uncertainty for a specific site.

The COVs in Table 6 are larger than the COVs of the transformation uncertainty for soil parameters

(Ching and Phoon 2014b; Ching et al. 2017b). This suggests that the site challenge is more significant for rock engineering than geotechnical engineering. Research in developing data-driven methods that are effective in producing useful insights from real world data is only emerging in geotechnical engineering. Comparable research in rock engineering is apparently limited (Harrison 2019).

CONSTRUCTION OF QUASI-SITE-SPECIFIC MODEL – ILLUSTRATION

Given that existing E_m transformation models may be inaccurate for a specific site, it is desirable to construct a site-specific transformation model. However, a site-specific model is plagued by large statistical uncertainties if the site-specific data are sparse. In this circumstance, a quasi-site-specific model that is supported by relevant data from a generic database can be useful. In this section, the construction of a quasi-site-specific transformation model supported by ROCKMass/9/5876 is illustrated. To explain the site challenge and the proposed solutions clearly and visually, a two-dimensional (2-D) bivariate model considering only two rock mass properties Y_2 = RMR and Y_5 = $\ln(E_m)$ is first discussed. The construction of a high-dimensional multivariate model will be presented later.

For illustration, this section describes the construction of a quasi-site-specific model between Y_2 and Y_5 for a target site at the Artvin dam, Turkey. This site is not covered by ROCKMass/9/5876. The data for the Artvin dam site, shown in Table 7, are extracted from Kayabasi and Gokceoglu (2018). The target-site dataset in Table 7 is denoted by D_s, whereas ROCKMass/9/5876 is denoted by D_g. In D_s, there are 34 tuff rock mass cases with E_m determined by plate-loading tests. The RMR-

E_m data are shown in Figure 4a. Four methods of constructing a probabilistic quasi-site-specific transformation model for $Y_5 = \ln(E_m)$ versus Y_2 = RMR are investigated. They are the probabilistic multiple regression (PMR), hybridization (HYB), hierarchical Bayesian model (HBM), and similarity method (SIM). Only the E_m values for the 1st, 17th, and 32nd cases are treated as known during the analysis (red circles in the figure), and those for the remaining 31 cases are treated as unknown (yellow circles in the figure). The 3 cases are selected because their RMR values spanned a wide range (RMR = 51, 72, and 30). This wide range of RMR is desirable from the viewpoint of statistical experimental design. A sensitivity study indicates that a narrow range of these RMR values may cause the inference results for HYB and SIM to be less stable.

For all four methods, a quasi-site-specific probabilistic transformation model is first constructed by D_g and/or D_s with 31 E_m values treated as unknown. In other words, the E_m column in Table 7 only contains 3 values at rows 1, 17, and 32. Using this column censored Table 7 as site-specific data (labelled as D_{sc}), a quasi-site-specific model is constructed with the support of D_g. The constructed model is then used to infer the unknown E_m values of the 31 cases. Because the Artvin dam site is not covered by ROCKMass/9/5876, the inference results (e.g., whether the 31 actual E_m values are contained by the 95% confidence interval) represent a genuine validation of the proposed methods.

Probabilistic multiple regression

The probabilistic multiple regression (PMR) was first proposed by Ching and Phoon (2012) and was subsequently implemented by Ching and Phoon (2014a), Ching et al. (2014, 2017a, 2019), Liu et al. (2016), Zou et al. (2017), and Zhang et al. (2020). The basic idea is to first convert the physical (Y_2,

Y_5) database into a standard normal (X_2, X_5) database using Eq. (2.) and then construct the bivariate normal probability density function (PDF) of (X_2, X_5) based on this standard normal database. The constructed PDF, denoted by $f(x_2, x_5|D_g)$ (the contour lines in Figure 5a), is regarded as the generic model. This generic model is adopted as the prior model. It is updated into the posterior model, denoted by $f(x_5|x_2,D_g)$, based on the site-specific x_2 information using Bayesian analysis. The posterior model in the standard normal space $f(x_5|x_2,D_g)$ is converted back to the version in the physical space $f(y_5|y_2,D_g)$ by the inverse function of Eq. (2.), and $f(y_5|y_2,D_g)$ is regarded as the quasi-site-specific model produced by PMR.

Consider No. 2 case in Table 7 (E_m is unknown) as an example. Conditioning its y_2 = RMR = 65 information, the posterior PDF $f(y_5|y_2 = 65,D_g)$ can be obtained by Bayesian analysis, and the median and 95% confidence interval of Y_5 are shown in Figure 5b (95% CI is the vertical bar, whereas the median is the small horizontal tick). For this case, its $Y_5 = E_m$ value is observed, although treated as unknown during analysis. The vertical coordinate of the yellow circle in Figure 5b indicates its observed E_m value. It is desirable that the yellow circle is within the 95% CI. There are 31 cases with unknown E_m. The inference results for all 31 cases are shown in Figure 5c.

The main assumption for PMR is that the site-specific data in D_{sc} follow the PDF for the generic data in D_g. This assumption is reasonable if D_{sc} is a plausible realization of D_g. However, this assumption may not hold because D_{sc} usually occupies a range narrower than D_g. In contrast to HYB, HBM, and SIM, PMR does not construct a site-specific PDF. It is also crucial to note that the quasi-site-specific model $f(y_5|y_2,D_g)$ only depends on site-specific y_2 (RMR) values for the 3 cases. The

site-specific y_5 [$\ln(E_m)$] values for the 3 cases have no effect on $f(y_5|y_2,D_g)$. As discussed later, this is the main pitfall of PMR.

Hybridization method

The hybridization method (HYB) was proposed by Ching and Phoon (2019). The basic idea is to first construct the generic model $f(x_2, x_5|D_g)$ as done in PMR (see Figure 6a). A site-specific model, denoted by $f(x_2, x_5|D_{sc})$, is also constructed based on the site-specific data using a Gibbs sampler (see Figure 6b). Then, a so-called hybrid PDF, denoted by $f_h(x_2, x_5)$, is proportional to the direct product between $f(x_2, x_5|D_g)$ and $f(x_2, x_5|D_{sc})$ (see Figure 6c). This hybrid PDF is converted back to its version in the physical space $f_h(y_2, y_5)$ by the inverse function of Eq. (2.) (see Figure 6d). The posterior PDF $f_h(x_5|x_2)$ can be computed by Bayesian analysis, and $f_h(x_5|x_2)$ is regarded as the quasi-site-specific model. For each of the 31 cases in D_{sc} with unknown E_m, the median and 95% CI for $f_h(y_5|y_2)$ are computed. The inference results for all 31 cases are shown in Figure 6d. It is desirable that the yellow circles in Figure 6d are within the 95% CIs.

In contrast to PMR, HYB does not require the assumption that D_{sc} and D_g follow the same PDF. They can follow different PDFs. It is crucial to note that the quasi-site-specific model $f_h(y_5|y_2)$ not only depends on site-specific y_2 (RMR) values for the 3 cases but also depends on their site-specific y_5 [$\ln(E_m)$] values, because these y_5 values affects $f(x_2, x_5|D_{sc})$.

Hierarchical Bayesian model

The hybridization idea of multiplying two PDFs together is ad hoc because it is not based on rigorous probability theory. Ching et al. (2020) adopted a hierarchical Bayesian model (HBM) (Gelman and

Hill 2006; Zhang et al. 2014, 2016; Lu et al. 2018; Bozorgzadeh et al. 2019; Bozorgzadeh and Bathurst 2020) to construct a quasi-site-specific model based on rigorous probability theory. In this approach, only the RMR-E_m data points in D_g with group information can be used. There are 39 such RMR-E_m data groups in D_g, but only 23 data groups with 3 or more RMR-E_m data points are adopted in the current example. The cases for these 23 groups are shown in Figure 4b, where the cases from the same group are annotated by the same label. The (X_2, X_5) data for the i-th group are assumed to follow a certain bivariate normal PDF with mean vector $\underline{\mu}_i = [\mu_{2i}\ \mu_{5i}]^T$ and covariance matrix $\mathbf{C}_i = [\sigma_{2i}^2\ \rho_i\sigma_{2i}\sigma_{5i};\ \rho_i\sigma_{2i}\sigma_{5i}\ \sigma_{5i}^2]$, where ($\mu_2$, μ_5) are the mean values of (X_2, X_5), (σ_2, σ_5) are their variances, and ρ_i is the correlation between X_2 and X_5. The site-specific data D_{sc} is also assumed to constitute a data group that follows a bivariate normal PDF with mean vector $\underline{\mu}_{sc}$ and covariance matrix $\mathbf{C}_{sc}$. A key assumption in HBM is that ($\underline{\mu}_1$, $\underline{\mu}_2$, … $\underline{\mu}_{23}$, $\underline{\mu}_{sc}$) are distinct but are identically distributed and that ($\mathbf{C}_1$, $\mathbf{C}_2$, …$\mathbf{C}_{23}$, $\mathbf{C}_{sc}$) are distinct but are also identically distributed. Because of the structure of identical distributions, D_g and ($\underline{\mu}_{sc}$,C_{sc}) are dependent, and it is possible to learn ($\underline{\mu}_{sc}$,C_{sc}) from D_g.

The basic idea of HBM is to first construct $f(\underline{\mu}_{sc},C_{sc}|D_g)$. This PDF is regarded as the prior model. The contour lines and histogram in Figure 7 show the resulting $f(\underline{\mu}_{sc},C_{sc}|D_g)$. In the figure, the actual statistics (μ_2, μ_5, σ_2, σ_5, and ρ) for the 23 data groups are shown as solid dots, with the number of cases annotated beside each dot. Then, $f(\underline{\mu}_{sc},C_{sc}|D_g)$ is updated into $f(\underline{\mu}_{sc},C_{sc}|D_g, D_{sc})$ based on D_{sc} by Bayesian analysis. The updated PDF $f(\underline{\mu}_{sc},C_{sc}|D_g, D_{sc})$ is shown as the contour lines and histogram in Figure 8, together with the statistics for D_{sc} shown as solid dots. $f(x_2, x_5|D_g, D_{sc})$ can be deduced from $f(\underline{\mu}_{sc},C_{sc}|D_g, D_{sc})$ based on the total probability theory (see Figure 9a). $f(x_2, x_5|D_g, D_{sc})$ is converted

back to its version in the physical space $f(y_2, y_5|D_g, D_{sc})$ by the inverse function of Eq. (2.). $f(y_5|y_2, D_g, D_{sc})$, regarded as the quasi-site-specific model, can be computed by Bayesian analysis (Figure 9b). For each of the 31 cases in D_{sc} with unknown E_m, the median and 95% CI for $f(y_5|y_2, D_g, D_{sc})$ are computed. The inference results for all 31 cases are shown in Figure 9b. It is desirable that the yellow circles in Figure 9b are within the 95% CIs.

The main assumption for HBM is that $\underline{\mu}_{sc}$ and $(\underline{\mu}_1, \underline{\mu}_2, \ldots \underline{\mu}_{23})$ are identically distributed, and $\mathbf{C}_{sc}$ and $(\mathbf{C}_1, \mathbf{C}_2, \ldots \mathbf{C}_{23})$ are also identically distributed. It is crucial to note that the quasi-site-specific model $f(y_5|y_2, D_g, D_{sc})$ not only depends on site-specific y_2 (RMR) values for the 3 cases but also depends on their site-specific y_5 $[\ln(E_m)]$ values.

Similarity method

The purpose for PMR, HYB, and HBM is to construct a quasi-site-specific model. Strictly speaking, the purpose for the similarity method (SIM) (Ching and Phoon 2020) is not to construct a quasi-site-specific model but to construct a quasi-site-specific dataset. First, SIM finds the cases in D_g that are similar to D_s in Table 7. All information (X_1, X_2, X_4, X_5), corresponding to RQD, RMR, GSI, and $\ln(E_m)$ in physical space, is used when quantifying the similarity. Second, these cases can be used to augment D_s to form a quasi-site-specific dataset in a suitably weighted manner according to the similarity. This weighted database can be adopted to construct a quasi-site-specific transformation model. The similarity index between a record in D_g and D_s is denoted by S. Figure 10a shows the S values for all cases in D_g: a darker dot indicates a case with higher S value. The quasi-site-specific dataset is formed by assigning a weight = 1 for each record in D_s and assigning a weight related to S

for each record in D_g. The weight for a record in D_g is close to 1 if the record is similar to D_s; zero otherwise. The quasi-site-specific dataset is used to construct the following linear regression model between X_2 and X_5:

$$X_5 = a + b \cdot X_2 + \varepsilon \quad (4.)$$

where (a, b) are regression coefficients; ε is a zero-mean normal variable with standard deviation = σ. The parameters (a, b, σ) are estimated by maximum likelihood based on the (X_2, X_5) data sampled from the quasi-site-specific dataset according to the weights. The resulting regression model represents the quasi-site-specific model constructed by SIM, and this regression model is converted back to the regression model for (Y_2, Y_5) by the inverse function of Eq. (2.). The median and 95% CI for Y_5 represent the inference result (see Figure 10b).

SIM does not make any assumption on whether D_g and D_s should follow the same distribution. It is crucial to note that the quasi-site-specific model not only depends on site-specific y_2 (RMR) values for the 3 cases but also depends on their site-specific y_5 [ln(E_m)] values.

Effect of more E_m tests

The above analysis results for PMR, HYB, HBM, and SIM are for the scenario of 3 E_m tests, denoted by n_{test} = 3. Figures 11a-11d summarize the inference results for n_{test} = 3. In this section, the effect of more E_m tests is investigated. In general, a dataset with more E_m tests (n_{test} = 10) is used to construct the quasi-site-specific model, and the model is used to infer the remaining 34-10 = 24 E_m values. Figures 12a-12d summarize the inference results for PMR, HYB, HBM, and SIM, respectively, for n_{test} = 10. The red circles in these figures are the cases with observed E_m, whereas the yellow circles

are the cases whose E_m values are to be inferred. Each yellow circle is associated with a 95% CI (vertical bar). Figure 13 compares the median estimates for PMR, HYB, HBM, and SIM with the measured E_m values on a 1:1 plot. The following observations are obtained:

1. The 95% CIs for PMR are not reduced by adding more E_m test values to D_{sc}, whereas those for HYB, HBM, and SIM are reduced. This is because PMR constructs a model that only depends on D_g as well as RMR values in D_{sc}. Increasing E_m tests in D_{sc} has no effect on PMR.
2. In Figure 11, PMR produces the widest 95% CI, HYB produces the second widest, SIM produces the second narrowest, and HBM produces the narrowest. The width of the 95% CI quantifies the transformation uncertainty. In Figure 13, PMR produces median estimates that are farthest away from the 1:1 line, HYB and SIM produce the second farthest, and HBM produces the nearest. The distance to the 1:1 line quantifies the transformation bias. As a result, the ranking for effectiveness in terms of transformation uncertainty and bias is HBM > SIM > HYB > PMR (“>” means more effective) for this particular site. This ranking is more evident when the number of E_m tests is small (e.g., $n_{test} = 3$).

Effect of a different input variable

The above results are for the RMR-E_m transformation model. A different input variable may lead to different results. Figure 14 shows the inference result if the input variable is different. Only the HBM results are illustrated herein because HBM is likely to be the most effective. Figures 14b and 14c show the inference results for HBM if the input variable RMR is replaced by GSI and RQD. For this particular case study, the RMR information is more effective than GSI and RQD in terms of

transformation uncertainty, because the 95% CIs in Figure 14a are narrower than those in Figures 14b and 14c. For a bivariate model to be effective, it is essential to select a proper input variable. A poor selection can lead to large transformation uncertainty. Nonetheless, the advantage of a probabilistic approach compared to a deterministic approach is that an engineer is automatically informed of the quality of any transformation model by the size of the 95% CI.

It is possible is to incorporate multiple input variables to construct a multivariate model that could lead to a smaller 95% CI. A multivariate model can relieve the engineer from choosing the "best" input variable – a task that come with a conventional bivariate model that admits only one input variable. For the current case study, this means that (RMR, GSI, RQD) are all taken to be predict E_m. The construction for a multivariate probabilistic transformation is illustrated in the next section.

Multivariate probabilistic transformation model – second case study

A second case study not within ROCKMass/9/5876, the İzmir subway site in Turkey, is analyzed in this section to illustrate the effect of incorporating multiple input variables. The data are extracted from Kıncal and Koca (2019), shown in Table 8. There are 32 andesitic rock mass cases whose E_m values were determined by borehole (pressuremeter) tests. To incorporate multiple inputs, the following 7 models (M1~M7) are considered:

1. (M1~M4) E_m probabilistic transformation models with a single input RQD (M1), RMR (M2), E_i (M3), or σ_{ci} (M4). These are bivariate models. Note that M2 is exactly the RMR-E_m transformation model investigated in the previous section.
2. (M5) Model with 2 inputs (RQD, E_i), a 3-D multivariate model.

3. (M6) Model with 3 inputs (RQD, E_i, σ_{ci}), a 4-D multivariate model.

4. (M7) Model with 4 inputs (RQD, RMR, E_i, σ_{ci}), a 5-D multivariate model.

Only PMR, HYB, and HBM are investigated, whereas SIM is not. For a multivariate model such as M5, M6, and M7, SIM requires a sufficient number of multivariate D_g cases with 3 or more parameters known. As seen in Table S1 in the supplementary material, although there are abundant bivariate cases (two parameters known) in ROCKMass/9/5876, there are not many multivariate cases (3 or more known). As a result, SIM is not investigated. This can be regarded as a limitation of SIM compared to PMR, HYB and HBM. Note that PMR, HYB, and HBM can still construct a multivariate model even if D_g is dominated by bivariate cases. The steps for constructing a high-dimensional multivariate model (M5, M6, or M7) for PMR, HYB, and HBM are the same as those for constructing a bivariate model. Although D_g is dominated by bivariate cases, PMR, HYB, and HBM are still applicable because they use the GS method, and the GS method can handle incomplete data.

For illustration, only the E_m values for the 10^{th}, 16^{th}, and 22^{nd} cases in Table 8 are treated as known during the analysis, and those for the remaining 29 cases are treated as unknown. These 3 cases are selected because their values cover a wide range (see the red circles in Figure 15). A probabilistic quasi-site-specific transformation model is first constructed with 29 E_m values treated as unknown. The constructed model is then used to infer the E_m values of the 29 cases. Because the İzmir subway site is not covered by ROCKMass/9/5876, the inference results represent a genuine validation of the proposed methods. Figure 16 shows the inference results for PMR, HYB, and HBM for Case No. 1 in Table 8. The 7 vertical bars show the 95% CIs produced by M1~M7, whereas the

yellow circles indicate the observed E_m value (treated as unknown during analysis). The following observations are obtained:

1. HBM produces the narrowest 95% CI and least bias, so it is the most effective in terms of transformation uncertainty and bias. PMR is the least effective, and HYB is the intermediate.
2. For the models with a single input (M1~M4), (M2, M3) usually produce narrower 95% CIs than (M1, M4). This suggests that the (RMR, E_i) information is more effective than (RQD, σ_{ci}) in terms of transformation uncertainty.
3. The models with multiple inputs (M5, M6, and M7) usually produce narrower 95% CIs and lesser bias than those with a single input (M1~M4). Moreover, M7 is usually the most effective.
4. In Figure 16a (for PMR), the E_m value for Case No. 1 is not within the 95% CI for M3. This inconsistency also happens for many other cases. This inconsistency is due to the fact that the E_i-E_m trend in Table 9 are not well covered by the E_i-E_m data cloud in D_g. The situation is improved by adopting HYB and HBM (Figures 16b and 16c), as the E_m value is now within the 95% CI for M3. The improvement is due to the fact that the models constructed by HYB and HBM are affected by the observed E_m values in Table 9. The improvement is especially clear for HBM (Figure 16c), as the E_m value is now well within the 95% CI for M3.

Figure 16 is only for Case No. 1. Figure 17 shows the inference results for all 29 cases. For each case, the 7 vertical bars indicate the 95% CIs for M1~M7. It is evident that the above observations #1~#4 still hold for all cases in general.

CONCLUSIONS

It is found that E_m correlation trends such as the RMR-E_m relationship are strongly site-specific so that a generic E_m transformation model may not be effective in predicting site-specific E_m. This is to be expected, because a generic model incorporates all available data without regard to site-specific differences. A better model is possible if the engineer is familiar with all the sites in the generic database and can manually weed out less relevant records manually based on his/her experiences. This is widely known in current practice.

In principle, a purely site-specific model is the most accurate. However, many projects conduct a limited number of E_m tests. As a result, a site-specific E_m transformation model cannot be constructed and engineers are frequently left with no option but to adopt less effective generic models proposed in the literature. As noted above, some engineers may improve on this state of the practice by combining site-specific data and a generic database for regression analysis. Engineers with sufficient experience may identify some sites in the generic database as more "similar" and restrict their analysis to those sites. This state of the practice (using models directly from the literature or to improve them with site-specific data) is limited in three ways: (1) raw data supporting a generic model may not be made available (not uncommon in the literature), (2) site-specific data are usually overwhelmed by the generic database because of their sparsity and (3) engineering judgment is needed to identify "similar" sites, but judgment cannot be applied beyond an engineer's experience base and is arguably not feasible when the database becomes very large. In response to (1), this paper compiles a new generic database for rock mass parameters named ROCKMass/9/5876. In response

to (2), this paper constructs quasi-site-specific transformation models for E_m that are least biased and most precise *for any given site*. Reducing bias can only be achieved by weighing site-specific data and generic data more appropriately. Increasing precision will require limited site-specific data to be augmented by a much larger generic database. In response to (3), algorithms that can account for site-specific differences in the generic data are studied.

The generic rock mass database (ROCKMass/9/5876) consists of 9 parameters (RQD, RMR, Q, GSI, E_m, E_{em}, E_{dm}, E_i, σ_{ci}). This database is shown to cover a wide range of conditions. There is no strong evidence indicating that the transformation relationship exhibited by ROCKMass/9/5876 depends on rock class or the E_m test type. As to be expected, the data scatter for ROCKMass/9/5876 about the mean correlation trend at this generic level is quite significant.

The feasibility of constructing a quasi-site-specific probabilistic E_m transformation model is investigated. With ROCKMass/9/5876, it is possible to construct a useful quasi-site-specific model even if the site-specific data are sparse (e.g., only 3 E_m tests are conducted). Four methods are investigated: probabilistic multiple regression (PMR), hybridization method (HYB), hierarchical Bayesian method (HBM), and similarity method (SIM). The analysis results for two real case studies in Turkey (Artvin dam site and İzmir subway site) indicate the following:

1. The transformation uncertainty and bias for HYB, HBM, and SIM can be reduced by conducting more site-specific E_m tests, whereas this reduction is not achieved for PMR even in the presence of more site-specific tests.
2. The ranking for effectiveness in terms of achieving least transformation uncertainty and bias is

HBM > SIM > HYB > PMR (">" means more effective).

3. Incorporating more input variables may further reduce the transformation uncertainty and bias. This implies that the use of all measured parameters in the form of a multivariate quasi-site-specific model is more effective than the common bivariate model. The details for constructing of multivariate models can be found in Ching and Phoon (2015).

The illustrations in this paper focus on the construction of a quasi-site-specific model that predicts E_m. The same steps given in this paper can be used to construct a model that predicts other parameters in ROCKMass/9/5876, such as E_{em} (elastic modulus of a rock mass).

ACKNOWLEDGMENTS

The first author would like to thank the Ministry of Science and Technology of Taiwan for the gracious funding support (106-2221-E-002-084-MY3 and 107-2221-E-002-053-MY3).

DATA AVAILABILITY

The rock mass database ROCKMass/9/5876 can be downloaded at the following ISSMGE TC304 (risk) webpage: http://140.112.12.21/issmge/tc304.htm?=6. The computer codes generated in this study are available from the corresponding author on reasonable request.

REFERENCES

Ajalloeian, R. and Mohammadi, M. 2014. Estimation of limestone rock mass deformation modulus

using empirical equations. Bulletin of Engineering Geology and the Environment, 73(2), 541-550.

Aladejare, A.E. and Wang, Y. 2017. Evaluation of rock property variability. Georisk: Assessment and Management of Risk for Engineered Systems and Geohazards, 11(1), 22-41.

Barton, N. 1995. Permanent support for tunnels using NMT—Special Lecture. In Proc. Symp. Of KRMS (Korea Rock Mechanics Society) and KSEG (Korea Society of Engineering Geology), 1-26.

Barton, N. 2002. Some new Q-value correlations to assist in site characterisation and tunnel design. International Journal of Rock Mechanics and Mining Sciences, 39(2), 185-216.

Barton, N., Lien, R., and Lunde, J. 1974. Engineering classification of rock masses for the design of tunnel support. Rock Mechanics, 6(4), 189-236.

Beiki, M., Bashari, A., and Majdi, A. 2010. Genetic programming approach for estimating the deformation modulus of rock mass using sensitivity analysis by neural network. International Journal of Rock Mechanics and Mining Sciences, 47(7), 1091-1103.

Bieniawski, Z.T. 1973. Engineering classification of jointed rock masses. Transactions of the South African Institution of Civil Engineers. 15, 335-344.

Bieniawski, Z.T. 1976. Rock mass classification in rock engineering. In: Bieniawski, Z.T. (Ed.), Proc. Symp. on Exploration for Rock Eng., 1, 97-106.

Bieniawski, Z.T. 1978. Determining rock mass deformability: Experience from case histories. International Journal of Rock Mechanics and Mining Sciences, 15, 237-247.

Bozorgzadeh, N. and Bathurst, R.J. 2020. Hierarchical Bayesian approaches to statistical modelling of geotechnical data. Georisk, in review.

Bozorgzadeh, N., Harrison, J. P. and Escobar, M. D. 2019. Hierarchical Bayesian modelling of geotechnical data: application to rock strength. Géotechnique, 69(12), 1056-1070.

Ching, J. 2018. What does the soil parameter estimated from a transformation model really mean? Journal of GeoEngineering, 13(3), 105-113.

Ching, J. and Phoon, K. K. 2015. Constructing multivariate distributions for soil parameters. Chap. 1 in Risk and Reliability in Geotechnical Engineering (Eds.: K.K. Phoon and J. Ching). Taylor & Francis.

Ching, J. and Phoon, K.K. 2012. Modeling parameters of structured clays as a multivariate normal distribution. Canadian Geotechnical Journal, 49(5), 522-545.

Ching, J. and Phoon, K.K. 2013. Multivariate distribution for undrained shear strengths under various test procedures. Canadian Geotechnical Journal, 50(9), 907-923.

Ching, J. and Phoon, K.K. 2014a. Correlations among some clay parameters – the multivariate distribution. Canadian Geotechnical Journal, 51(6), 686-704.

Ching, J. and Phoon, K.K. 2014b. Transformations and correlations among some parameters of clays – the global database. Canadian Geotechnical Journal, 51(6), 663-685.

Ching, J. and Phoon, K.K. 2019. Constructing site-specific multivariate probabilistic distribution model by Bayesian machine learning, ASCE Journal of Engineering Mechanics, 145(1), 04018126.

Ching, J. and Phoon, K.K. 2020. Measuring similarity between site-specific data and records from other sites. ASCE-ASME Journal of Risk and Uncertainty in Engineering Systems, Part A: Civil Engineering, 6(2), 04020011.

Ching, J., Li, K.H., Phoon, K.K., and Weng, M.C. 2018. Generic transformation models for some intact rock properties. Canadian Geotechnical Journal, 55(12), 1702-1741.

Ching, J., Lin, G.H., Chen, J.R., and Phoon, K.K. 2017b. Transformation models for effective friction angle and relative density calibrated based on a multivariate database of coarse-grained soils. Canadian Geotechnical Journal, 54(4), 481-501.

Ching, J., Lin, G.H., Phoon, K.K., and Chen, J.R. 2017a. Correlations among some parameters of coarse-grained soils – the multivariate probability distribution model, Canadian Geotechnical Journal, 54(9), 1203-1220.

Ching, J., Phoon, K.K., and Chen, C.H. 2014. Modeling CPTU parameters of clays as a multivariate normal distribution. Canadian Geotechnical Journal, 51(1), 77-91.

Ching, J., Phoon, K.K., Li, K.H., and Weng, M.C. 2019. Multivariate probability distribution for some intact rock properties, Canadian Geotechnical Journal, 56(8), 1080-1097.

Ching, J., Wu, S., and Phoon, K.K. 2020. Constructing quasi-site-specific multivariate probability distribution using hierarchical Bayesian model. ASCE Journal of Engineering Mechanics (in review).

Conover, W.J. 1999. Practical Nonparametric Statistics. 3rd edition, John Wiley and Sons, Inc., New York.

Coon, R.F. and Merritt, A.H. 1970. Predicting in situ modulus of deformation using rock quality indexes. In Determination of the In Situ Modulus of Deformation of Rock, ASTM International, 154-173.

Deere, D.U. 1964. Technical description of rock cores. Rock Mechanics Engineering Geology, 1, 16-22.

D'Ignazio, M., Phoon, K.K., Tan, S.A., and Lansivaara, T. 2016. Correlations for undrained shear strength of Finnish soft clays. Canadian Geotechnical Journal, 53(10), 1628-1645.

Feng, S. and Vardanega, P. J. 2019. A database of saturated hydraulic conductivity of fine-grained soils: probability density functions. Georisk: Assessment and Management of Risk for Engineered Systems and Geohazards, 13(4), 255-261.

Gelman, A. and Hill, J. 2006. Data Analysis Using Regression and Multilevel/Hierarchical Models. Cambridge University Press.

Gokceoglu, C., Sonmez, H., and Kayabasi, A. 2003. Predicting the deformation moduli of rock masses. International Journal of Rock Mechanics and Mining Sciences, 40(5), 701-710.

Grimstad E. and Barton N. 1993. Updating the Q-System for NMT. In: Proceedings of the international symposium on sprayed concrete-modern use of wet mix sprayed concrete for underground support, Oslo, Norwegian Concrete Association.

Harrison, J. 2019. Challenges in determining rock mass properties for reliability-based design. Proceedings of 7th International Symposium on Geotechnical Safety and Risk (ISGSR 2019), Dec 11-13, Taipei, Taiwan, 35-44.

Hoek, E. and Brown, E.T. 1997. Practical estimates of rock mass strength. International Journal of Rock Mechanics and Mining Science, 34, 1165-1186.

Hoek, E. and Diederichs, M.S. 2006. Empirical estimation of rock mass modulus. International Journal of Rock Mechanics and Mining Sciences, 43(2), 203-215.

Johnson, N.L. 1949. Systems of frequency curves generated by methods of translation. Biometrika, 36(1/2), 149-176.

Kayabasi, A. and Gokceoglu, C. 2018. Deformation modulus of rock masses: An assessment of the existing empirical equations. Geotechnical and Geological Engineering, 36(4), 2683-2699.

Keffeler, E.R. 2014. Measurement and prediction of in-situ weak rock mass modulus case studies from Nevada, Puerto Rico, and Iran. Ph.D. Dissertation, University of Nevada, Reno.

Kim, E. and Hunt, R. 2017. A public website of rock mechanics database from Earth Mechanics Institute (EMI) at Colorado School of Mines (CSM). Rock Mechanics and Rock Engineering, 50(12), 3245-3252.

Kıncal, C. and Koca, M.Y. 2019. Correlations of in situ modulus of deformation with elastic modulus of intact core specimens and RMR values of andesitic rocks: a case study of the İzmir subway line. Bulletin of Engineering Geology and the Environment, 78, 5281-5299.

Kootahi, K. and Moradi, G. 2017. Evaluation of compression index of marine finegrained soils by the use of index tests. Marine Georesources and Geotechnology, 35(4), 548-570.

Liu, S., Zou, H., Cai, G., Bheemasetti, B.V., Puppala, A.J., and Lin, J. 2016. Multivariate correlation among resilient modulus and cone penetration test parameters of cohesive subgrade soils.

Engineering Geology, 209, 128–142.

Lu, S., Zhang, J., Zhou, S., and Xu, A. 2018. Reliability prediction of the axial ultimate bearing capacity of piles: A hierarchical Bayesian method. Advances in Mechanical Engineering, 10(11), 1-11.

Nejati, H.R., Ghazvinian, A., Moosavi, S.A., and Sarfarazi, V. 2014. On the use of the RMR system for estimation of rock mass deformation modulus. Bulletin of Engineering Geology and the Environment, 73, 531-540.

Palmström, A. and Singh, R. 2001. The deformation modulus of rock masses - comparisons between in situ tests and indirect estimates. Tunnelling and Underground Space Technology, 16(2), 115-131.

Phoon, K.K. and Kulhawy, F.H. 1999a. Evaluation of geotechnical property variability. Canadian Geotechnical Journal, 36(4), 625-639.

Phoon, K.K. and Kulhawy, F.H. 1999b. Characterization of geotechnical variability. Canadian Geotechnical Journal, 36(4), 612-624.

Phoon, K. K. 2017. Role of reliability calculations in geotechnical design. Georisk: Assessment and Management of Risk for Engineered Systems and Geohazards, 11 (1), 4-21.

Phoon, K.K. 2020. The story of statistics in geotechnical engineering. Georisk: Assessment and Management of Risk for Engineered Systems and Geohazards, 14(1), 3-25.

Prakoso, W.A. 2002. Reliability-based Design of Foundations on Rock Masses for Transmission Line and Similar Structures. Ph.D. Dissertation, Cornell University, Ithaca, NY.

Serafim, J.L. and Pereira, J.P. 1983. Considerations on the geomechanical classification of Bieniawski. In: Proceedings of the symposium on engineering geology and underground openings, Lisboa, Portugal, 1133-1144.

Sousa, L.R., Leitao, N.S., and Monteiro, G. 1999. Observed behaviour of the structures for the power increase of the Miranda hydroelectric project. Proceedings of 9th ISRM Congress, Paris, 1603-1612.

Zhang, D. M., Y. Zhou, K. K. Phoon, and H. W. Huang. 2020. Multivariate probability distribution of Shanghai clay properties. Engineering Geology (in review).

Zhang, J., Juang, C.H., Martin, J.R., and Huang, H.W. 2016. Inter-region variability of Robertson and Wride method for liquefaction hazard analysis. Engineering Geology, 203, 191-203.

Zhang, J., Li, J.P., Zhang, L.M., Huang, H.W. 2014. Calibrating cross-site variability for reliability-based design of pile foundations. Computers and Geotechnics, 62, 154-163.

Zhang, L. 2016. Engineering Properties of Rocks, 2nd Edition. Elsevier Ltd., Cambridge, MA, USA.

Zhang, L. 2017. Evaluation of rock mass deformability using empirical methods – A review. Underground Space, 2(1), 1-15.

Zhang, L. and Einstein, H. H. 2004. Using RQD to estimate the deformation modulus of rock masses. International Journal of Rock Mechanics and Mining Sciences, 41(2), 337-341.

Zou, H., Liu, S., Cai, G., Puppala, A.J., and Bheemasetti, T.V. 2017. Multivariate correlation analysis of seismic piezocone penetration (SCPTU) parameters and design properties of Jiangsu quaternary cohesive soils. Engineering Geology, 228, 11-38.

Table 1 Soil/rock parameter databases.

	Database	Reference	Parameters of interest	# data points	# sites/ studies	% of completeness
Univariate	CLAY/16	Phoon and Kulhawy (1999b)	γ, γ_d, w_n, PL, LL, PI, LI, ϕ', s_u, s_u^{FV}, q_c, q_t, SPT-N, DMT (A, B), PMT p_L		a	
	SAND/11	Phoon and Kulhawy (1999b)	ϕ', D_r, q_c, SPT-N, DMT (A, B, I_D, K_D, E_D), PMT (p_L, E_{PMT})		b	
	ROCK/8	Prakoso (2002)	γ (or γ_d), n, R, S_h, σ_{bt}, I_s, σ_c, E		c	
	ROCK/13	Aladejare and Wang (2017)	ρ, G_s, I_{d2}, n, w_c, γ, R_L, S_h, σ_{bt}, I_{s50}, σ_c, E, ν		d	
Multivariate	CLAY/5/345	Ching and Phoon (2012)	LI, s_u, s_u^{re}, σ'_p, σ'_v	345	37 sites	100%
	CLAY/7/6310	Ching and Phoon (2013)	s_u from 7 different test procedures	6310	164 studies	17.7%
	CLAY/6/535	Ching et al. (2014)	s_u/σ'_v, OCR, q_{tc}, q_{tu}, $(u_2-u_0)/\sigma'_v$, B_q	535	40 sites	100%
	CLAY/10/7490	Ching and Phoon (2014b)	LL, PI, LI, σ'_v/P_a, σ'_p/P_a, s_u/σ'_v, S_t, q_{tc}, q_{tu}, B_q	7490	251 studies	34.1%
	FI-CLAY/7/216	D'Ignazio et al. (2016)	s_u^{FV}, σ'_v, σ'_p, w_n, LL, PL, S_t	216	24 sites	100%
	JS-CLAY/5/124	Liu et al. (2016)	M_r, q_c, f_s, w_n, γ_d	124	16 sites	100%
	JS-CLAY/7/372	Zou et al. (2017)	σ_v, σ'_v, q_{tc}, f_s/σ'_v, B_q, V_{s1}, s_u/σ'_v	372	25 sites	100%
	SAND/7/2794	Ching et al. (2017b)	D_{50}, C_u, D_r, σ'_v/P_a, ϕ', q_{t1}, $(N_1)_{60}$	2794	176 studies	60.0%
	EMI-ROCK/8/26000+	Kim and Hunt (2017)	σ_c, σ_{bt}, ρ, CAI, PPI, cohesion, direction shear, triaxial confining	26000+	-	-
	FG/5/1000	Kootahi and Moradi (2017)	e, w_n, LL, PI, C_c	1000	170 sites	100%
	ROCK/9/4069	Ching et al. (2018)	γ, n, R_L, S_h, σ_{bt}, I_{s50}, V_p, σ_{ci}, E_i	4069	184 studies	34.2%
	FG-KSAT/6/1358	Feng and Vardanega (2019)	e, k, LL, PL, PI, G_s	1358	33 studies	91.4%
	SH-CLAY/11/4051	Zhang et al. (2020)	LL, PI, LI, e, K_0, σ'_v/P_a, s_u/σ'_v, S_t, q_c/σ'_v	4051	50 sites	39.5%
	ROCKMass/9/5876	This study	RQD, RMR, Q, GSI, E_m, E_{em}, E_{dm}, E_i, σ_{ci}	5784	225 studies	29.3%

Note: ρ = density; ν = Poisson ratio; γ = unit weight; ϕ' = effective friction angle; σ'_p = preconsolidation stress; σ'_v = vertical effective stress; σ_{bt} = Brazilian tensile strength; σ_{ci} = uniaxial compressive strength of intact rock; γ_d = dry unit weight; $(N_1)_{60} = N_{60}/(\sigma'_v/P_a)^{0.5}$; $(u_2-u_0)/\sigma'_v$ = normalized excess pore pressure; B_q = pore pressure ratio = $(u_2-u_0)/(q_t-\sigma_v)$; CAI = Cerchar abrasivity index; C_c = compression index; C_u = coefficient of uniformity; D_{50} = median grain size; DMT (A, B, I_D, K_D, E_D) = dilatometer A & B readings, material index, horizontal stress index, modulus; D_r = relative density; e = void ratio; E_{dm} = dynamic modulus of rock mass; E_{em} = elasticity modulus of rock mass; E_i = Young's modulus of intact rock; E_m = deformation modulus of rock mass; f_s = sleeve frictional resistance; G_s = specific gravity; GSI = geological strength index; I_{d2} = slake durability index; I_s = point load strength index ($I_{s50} = I_s$ for diameter 50 mm); k = hydraulic conductivity; K_0 = at-rest lateral earth pressure coefficient; LI = liquidity index; LL = liquid limit; M_r = subgrade resilience modulus; n = porosity; N_{60} = corrected SPT-N; OCR = overconsolidation ratio; P_a = atmospheric pressure = 101.3 kPa; PI = plasticity index; PMT (p_L, E_{PMT}) = pressuremeter limit stress, modulus; PPI = punch penetration index; Q = Q-system; q_c = cone tip resistance; q_t = corrected cone tip resistance; $q_{t1} = (q_t/P_a)/(\sigma'_v/P_a)^{0.5}$; $q_{tc} = (q_t-\sigma_v)/\sigma'_v$ = normalized cone tip resistance; $q_{tu} = (q_t-u_2)/\sigma'_v$ = effective cone tip resistance; R = Schmidt hammer hardness (R_L = L-type Schmidt hammer hardness); RMR = rock mass rating; RQD = rock quality designation; S_h = Shore scleroscope hardness; SPT-N = standard penetration test blow count; S_t = sensitivity; s_u = undrained shear strength for clay; s_u^{FV} = field vane s_u; s_u^{re} = remoulded s_u; u_0 = hydrostatic pore pressure; V_p = P-wave velocity; V_s = S-wave velocity; $V_{s1} = V_s(P_a/\sigma'_v)^{0.25}$; w_n = water content.

a - The no. of data groups varies between 2 and 42 depending on the clay parameter. Statistics are calculated at the data group level. The average no. of data points/data group varies between 16 and 564. Details given in Tables 1-3, Phoon & Kulhawy (1999b).
b - The no. of data groups varies between 5 and 57 depending on the sand parameter. Statistics are calculated at the data group level. The average no. of data points/data group varies between 15 and 123. Details given in Tables 1-3, Phoon & Kulhawy (1999b).
c – The no. of data groups varies between 30 and 174 depending on the rock parameter with no differentiation of rock type [igneous (intrusive, extrusive, pyroclastic), sedimentary (clastic, chemical), metamorphic (foliated, non-foliated)]. Statistics are calculated at the data group level. The average no. of data points/data group varies between 3 and 161 for σ_c (Prakoso, 2017). Details given in Table 4.4, Prakoso (2002).
d – The no. of data groups varies between 2 and 47 depending on the rock parameter and rock type (igneous, sedimentary, or metamorphic). Statistics are calculated at the data group level. The average no. of data points/data group varies between 7 and 92. Details given in Tables 2-4, Aladejare and Wang (2017).

Table 2 Statistics of ROCKMass/9/5876 at the generic level.

Parameter	Number of tests (number of data groups)	Mean	COV	Min	Max
RQD	1380 (154)	62.5	0.48	0	100
RMR	3399 (162)	55.5	0.33	0	97
Q	1933 (139)	21.5	2.92	0.001	1000
GSI	871 (107)	47.2	0.34	8	100
E_m (GPa)	3212 (180)	9.99	1.15	0.0011	104
E_{em} (GPa)	1386 (72)	14.50	1.12	0.00014	121
E_{dm} (GPa)	466 (33)	31.78	0.60	0.0411	85
E_i (GPa)	592 (131)	29.81	0.95	0.24	278
σ_{ci} (MPa)	2071 (240)	74.07	0.78	0.15	318

Table 3 Summary statistics of ROCKMass/9/5876 at the site level (igneous rock mass).

Property	No. of data groups	No. of tests/group		Range of data	Property mean value		Property COV	
		Range	Mean		Range	Mean	Range	Mean
RQD	17	3-38	7.9	0-100	17.0-91.7	64.1	0.052-0.90	0.33
RMR	22	3-26	9.5	9-96	31.0-78.4	58.6	0.036-0.66	0.23
Q	23	3-38	11.9	0.003-217.2	0.43-74.3	16.0	0.11-2.97	0.95
GSI	10	3-20	6.5	25-80	38.2-75.7	52.2	0.018-0.36	0.13
E_m (GPa)	15	3-20	5.5	0.29-72.85	1.75-47.3	14.3	0.10-1.42	0.59
E_{em} (GPa)	9	3-18	8.0	0.008-49.05	2.01-31.2	16.1	0.32-1.00	0.57
E_{dm} (GPa)	1	4	4.0	11.5-48.2	26.8	26.8	0.62	0.62
E_i (GPa)	9	3-11	5.1	2.3-105.8	13.5-79.2	37.5	0.032-0.99	0.42
σ_{ci} (MPa)	15	3-24	7.5	4.0-300	39.7-236.7	109.8	0.13-0.92	0.45

Table 4 Summary statistics of ROCKMass/9/5876 at the site level (sedimentary rock mass).

Property	No. of data groups	No. of tests/group		Range of data	Property mean value		Property COV (%)	
		Range	Mean		Range	Mean	Range	Mean
RQD	27	3-30	8.5	0-100	7.9-98.0	56.0	0.032-1.15	0.39
RMR	37	3-66	11.8	5-82	18.7-75.5	48.1	0.052-0.92	0.25
Q	22	3-49	13.0	0.005-70.0	0.3-19.8	6.2	0.29-1.76	0.88
GSI	21	3-29	8.4	8-86	24.0-73.3	41.5	0.059-0.58	0.29
E_m (GPa)	27	3-73	13.4	0.0011-57	0.12-29.7	9.3	0.13-1.25	0.68
E_{em} (GPa)	15	3-19	6.3	0.015-92.2	0.13-55.7	12.1	0.28-1.10	0.67
E_{dm} (GPa)	7	3-21	7.9	1.8-73.9	8.6-58.4	27.0	0.082-0.62	0.29
E_i (GPa)	14	3-52	9.1	1-89	4.3-76.0	23.2	0.083-1.20	0.45
σ_{ci} (MPa)	38	3-49	8.4	0.19-283.9	3.03-203.3	59.2	0.051-1.44	0.52

Table 5 Summary statistics of ROCKMass/9/5876 at the site level (metamorphic rock mass).

Property	No. of data groups	No. of tests/group		Range of data	Property mean value		Property COV (%)	
		Range	Mean		Range	Mean	Range	Mean
RQD	15	3-33	6.7	0-100	25.0-81.9	60.7	0.090-0.98	0.34
RMR	15	3-52	12.1	12-96	35.0-73.3	51.7	0.13-0.39	0.28
Q	17	3-60	13.2	0.001-636	0.14-44.8	9.7	0.13-4.61	1.34
GSI	4	3-11	7.3	17-70	23.8-55.0	43.6	0.063-0.32	0.20
E_m (GPa)	9	3-24	8.4	0.26-35.9	0.71-17.2	5.9	0.27-0.72	0.48
E_{em} (GPa)	3	5-24	11.3	1.4-26.8	2.4-9.8	6.0	0.38-0.55	0.46
E_{dm} (GPa)	2	5-5	5	1.8-26.0	2.9-18.7	10.8	0.30-0.45	0.37

E_i (GPa)	7	3-18	6.9	1.0-171.7	8.6-92.8	45.3	0.077-0.82	0.36
σ_{ci} (MPa)	9	3-18	8.6	3.0-187.8	33.5-177.2	81.3	0.058-0.85	0.49

Table 6 Some existing transformation models for E_m

Literature	Transformation model	Application range	Calibration results by ROCKMass/9/5876		
			No. data points (No. data groups)	b	δ
Coon and Merritt (1970)	$E_m/E_i = 0.0231\times RQD - 1.32$	RQD: 57~100	147 (10)	1.26	1.09
Zhang and Einstein (2004)	$E_m/E_i = 10^{0.0186\times RQD - 1.91}$	RQD: 0~100	161 (12)	1.54	0.89
Bieniawski (1978)	$E_m\,(GPa) = 2\times RMR - 100$	RMR: 50~85	1091 (26)	0.57	1.48
Gokceoglu et al. (2003)	$E_m\,(GPa) = 0.0736\times e^{0.0755\times RMR}$	RMR: 20~85	1749 (31)	1.53	1.21
Serafim and Pereira (1983)	$E_m\,(GPa) = 10^{(RMR-10)/40}$	RMR: 20~85	1749 (31)	0.51	1.00
Grimstad and Barton (1993)	$E_m\,(GPa) = 25\times \log_{10}(Q)$	Q: 1.1~1000	288 (13)	0.58	0.88
Palmström and Singh (2001)	$E_m\,(GPa) = 8\times Q^{0.4}$	Q: 1~30	35 (8)	0.37	0.56
Barton (2002)	$E_m\,(GPa) = 10\times\left[Q\times\sigma_{ci}\,(MPa)/100\right]^{1/3}$	Q: 1~100	36 (9)	0.32	0.45
Hoek and Diederichs (2006)	$E_m\,(GPa) = 100\times(1-D/2)\Big/\left[1+e^{(75+25D-GSI)/11}\right]$	GSI: 10~100	349 (17)	0.83 (D = 0)	1.00 (D = 0)
Beiki et al. (2010)	$E_m\,(GPa) = \tan\left(\left[1.56+\ln(GSI)^2\right]^{0.5}\right)\times\left[\sigma_{ci}\,(MPa)\right]^{1/3}$	GSI: 25~85	24 (8)	1.15	0.58
Hoek and Brown (1997)	$E_m\,(GPa) = 10^{(GSI-10)/40}\times\left[\sigma_{ci}\,(MPa)/100\right]^{1/2}$	σ_{ci} < 100 MPa	19 (7)	0.61	0.82

Table 7 Data for Artvin Dam site (extracted from Kayabasi and Gokceoglu 2018)

No.	RQD	RMR	Q	GSI	E_m (GPa)	E_{em} (GPa)	E_{dm} (GPa)	E_i (GPa)	σ_{ci} (MPa)
1	66	51	-	27	5.73	-	-	-	-
2	65	46	-	28	(2.57)	-	-	-	-
3	36	33	-	18	(4.47)	-	-	-	-
4	13	30	-	17	(4.71)	-	-	-	-
5	37	41	-	28	(5.82)	-	-	-	-
6	39	47	-	28	(12.46)	-	-	-	-
7	39	49	-	33	(12.66)	-	-	-	-
8	90	59	-	43	(8.34)	-	-	-	-
9	39	45	-	31	(12.12)	-	-	-	-
10	39	46	-	31	(10.67)	-	-	-	-
11	61	42	-	21	(7.39)	-	-	-	-
12	37	36	-	17	(3.44)	-	-	-	-
13	65	57	-	31	(11.54)	-	-	-	-
14	40	52	-	28	(8.17)	-	-	-	-
15	39	46	-	23	(13.14)	-	-	-	-
16	34	44	-	22	(11.10)	-	-	-	-
17	73	72	-	47	20.16	-	-	-	-
18	91	66	-	37	(16.15)	-	-	-	-
19	27	38	-	22	(1.57)	-	-	-	-
20	31	36	-	16	(2.51)	-	-	-	-
21	25	30	-	15	(1.77)	-	-	-	-
22	27	43	-	32	(3.61)	-	-	-	-
23	88	49	-	28	(7.44)	-	-	-	-
24	88	49	-	28	(12.08)	-	-	-	-
25	68	50	-	32	(8.57)	-	-	-	-
26	42	56	-	39	(13.31)	-	-	-	-
27	30	52	-	42	(12.10)	-	-	-	-
28	91	63	-	55	(12.96)	-	-	-	-
29	72	67	-	49	(19.16)	-	-	-	-
30	28	46	-	38	(9.71)	-	-	-	-
31	69	55	-	43	(8.85)	-	-	-	-
32	24	30	-	15	3.81	-	-	-	-

33	63	50	-	31	(6.21)	-	-	-	-
34	63	49	-	31	(5.48)	-	-	-	-

Table 8 Data for İzmir subway site (extracted from Kıncal and Koca 2019)

No.	RQD	RMR*	Q	GSI	E_m (GPa)	E_{em} (GPa)	E_{dm} (GPa)	E_i (GPa)	σ_{ci} (MPa)
1	5	25.5	-	-	(0.11)	-	-	4.2	26.0
2	18	35	-	-	(0.238)	-	-	7.0	39.5
3	32	41.5	-	-	(0.83)	-	-	10.8	72.0
4	35	41	-	-	(0.564)	-	-	9.0	62.0
5	37.4	41	-	-	(0.72)	-	-	10.7	65.2
6	24	36	-	-	(0.46)	-	-	10.0	50.0
7	40	39	-	-	(0.51)	-	-	8.0	61.0
8	18	35	-	-	(0.47)	-	-	8.5	48.5
9	34	35	-	-	(0.39)	-	-	7.5	51.2
10	42.5	44.5	-	-	1.17	-	-	12.3	86.4
11	45	45	-	-	(1.46)	-	-	13.0	90.0
12	42	43	-	-	(1.09)	-	-	14.4	81.3
13	27.5	36	-	-	(0.366)	-	-	7.5	57.3
14	20	36	-	-	(0.439)	-	-	8.7	54.0
15	25	37	-	-	(0.464)	-	-	10.0	60.0
16	23	35	-	-	0.336	-	-	9.3	53.7
17	20	34	-	-	(0.322)	-	-	9.0	53.0
18	20	33	-	-	(0.36)	-	-	9.25	53.4
19	11	37	-	-	(0.384)	-	-	9.66	58.1
20	21.5	27	-	-	(0.278)	-	-	6.5	37.1
21	10	20	-	-	(0.112)	-	-	4.33	14.3
22	4	19.5	-	-	0.11	-	-	4.0	23.0
23	32	26	-	-	(0.29)	-	-	6.8	27.4
24	30	34	-	-	(0.36)	-	-	6.4	37.0
25	16	32	-	-	(0.32)	-	-	8.0	40.2
26	12	29	-	-	(0.228)	-	-	6.0	30.2
27	28	30.5	-	-	(0.25)	-	-	7.33	37.2
28	14	31	-	-	(0.168)	-	-	4.4	29.0
29	43	45	-	-	(1.32)	-	-	11.5	85.6
30	41.5	38	-	-	(0.98)	-	-	9.58	70.5
31	26	43	-	-	(0.768)	-	-	10.5	71.2
32	13	33.5	-	-	(0.17)	-	-	5.33	35.0

* Average of the lower and upper bounds of RMRs reported in Kıncal and Koca (2019)

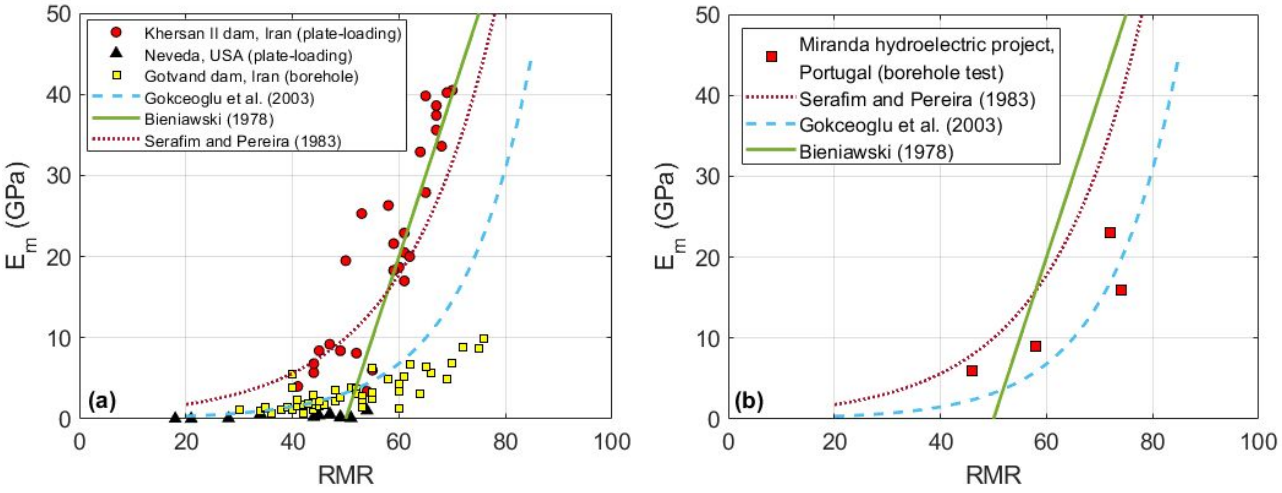

Figure 1 Relationship between RMR and E_m: (a) three construction sites; (b) a Portugal site.

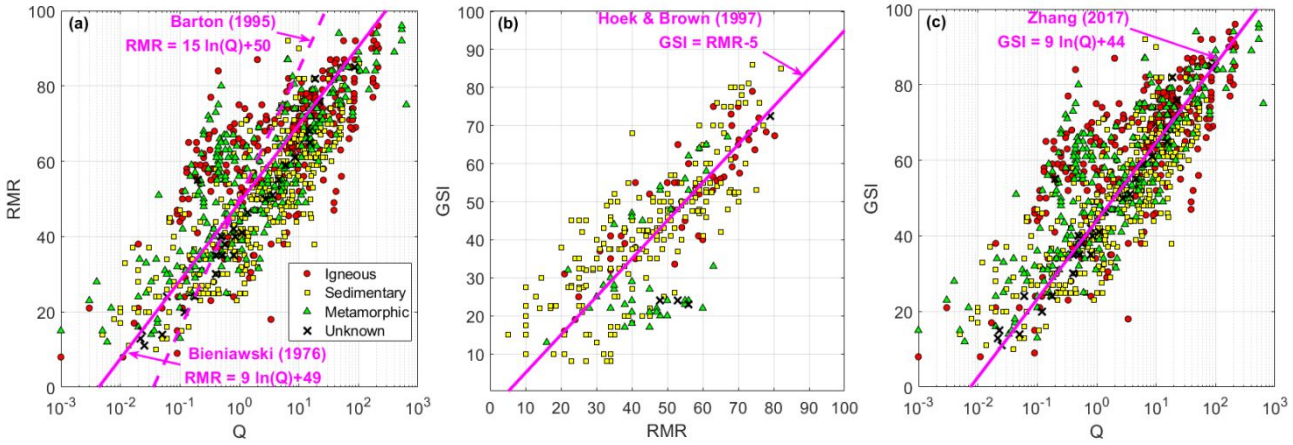

Figure 2 Relationships between (a) RMR & Q, (b) GSI & RMR, and (c) GSI & Q.

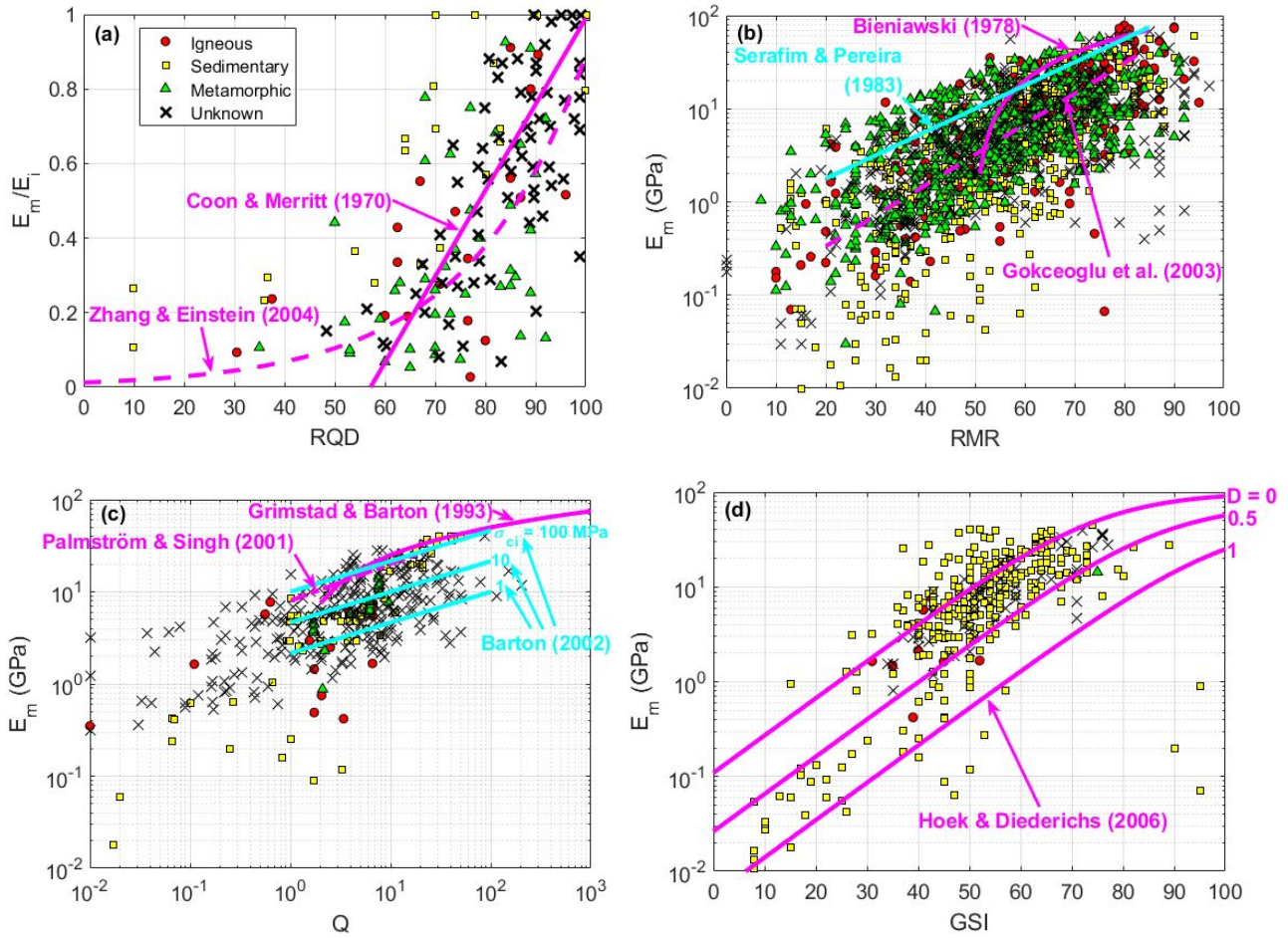

Figure 3 Relationships between (a) E_m/E_i & RQD, (b) E_m & RMR, (c) E_m & Q, and (d) E_m & GSI.

Submitted to ***Canadian Geotechnical Journal***

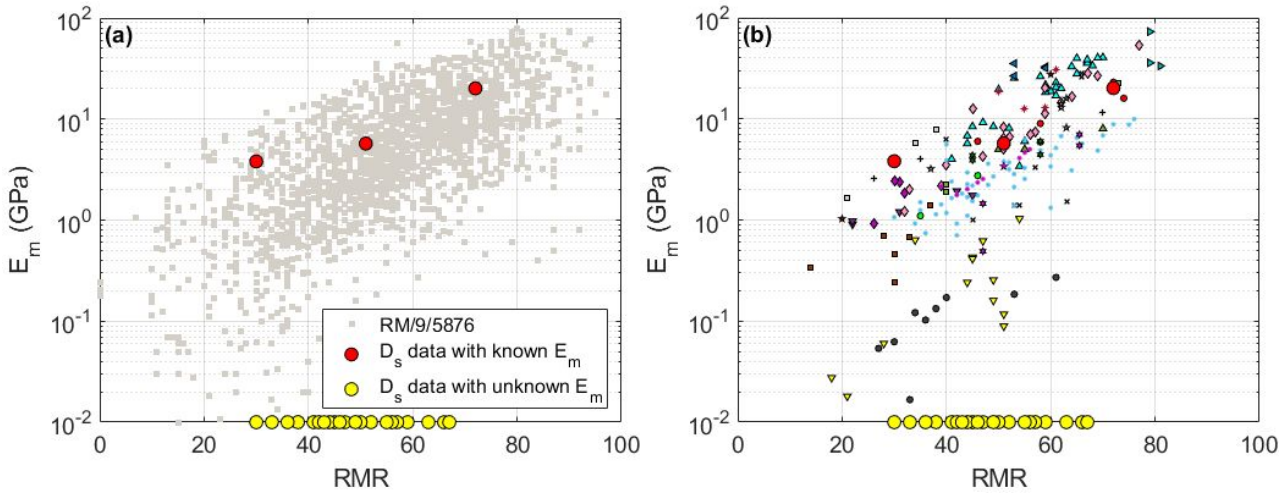

Figure 4 Data for Artvin Dam site: (a) without data groups; (b) with data groups.

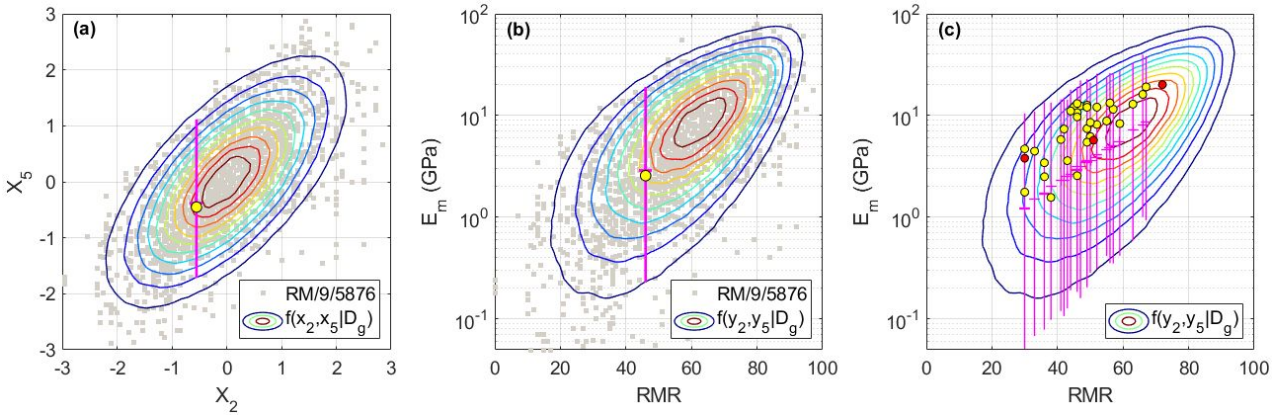

Figure 5 Illustration for PMR: (a) $f(x_2, x_5|D_g)$; (b) $f(y_2, y_5|D_g)$; (c) inference results for all 31 cases.

Submitted to ***Canadian Geotechnical Journal***

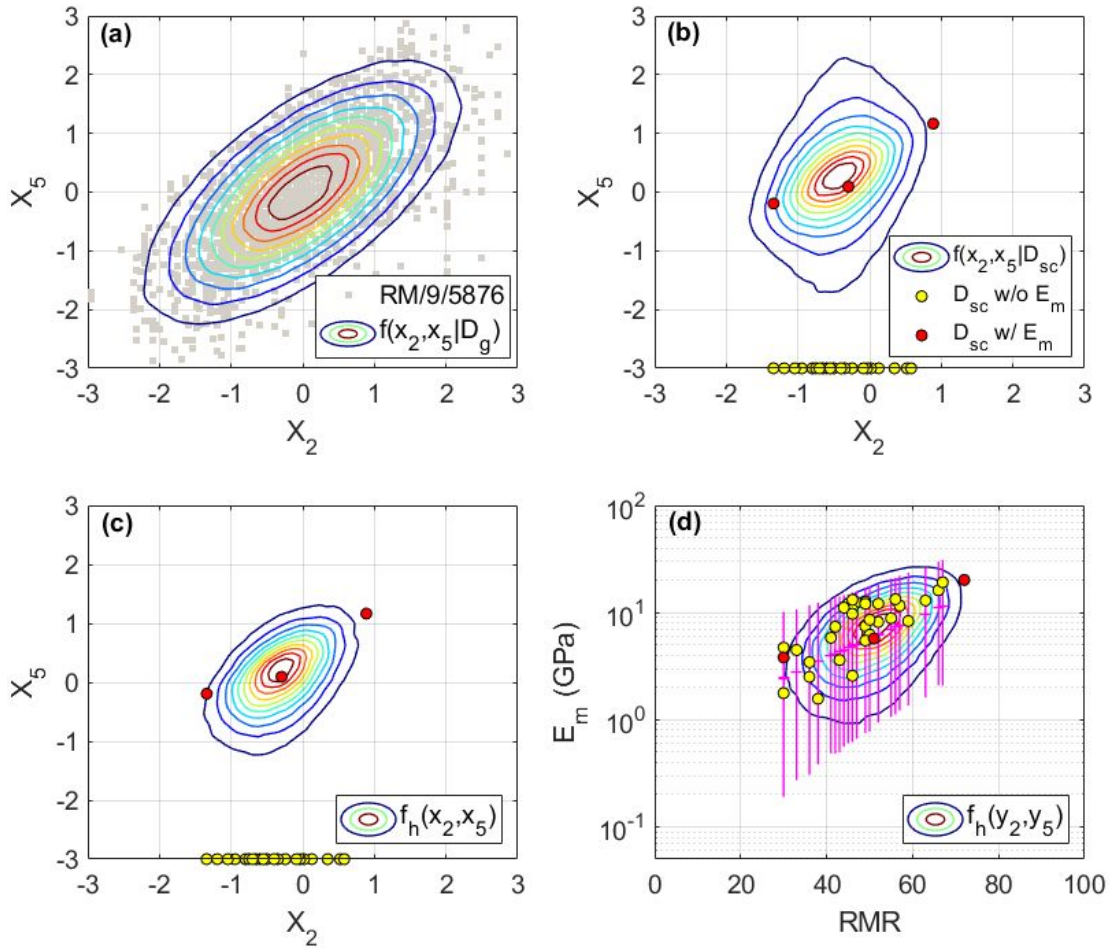

Figure 6 Illustration for HYB: (a) $f(x_2, x_5|D_g)$; (b) $f(x_2, x_5|D_{sc})$; (c) inference results in X space; (d) inference results.

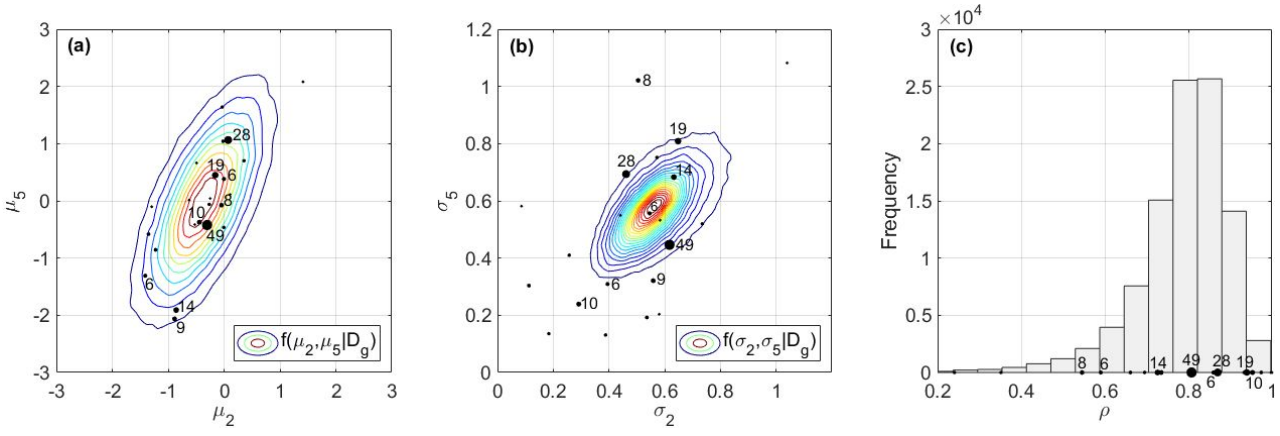

Figure 7 Illustration for $f(\underline{\mu}_{sc},\mathbf{C}_{sc}|D_g)$: (a) $f(\mu_2, \mu_5|D_g)$; (b) $f(\sigma_2, \sigma_5|D_g)$; (c) $f(\rho|D_g)$.

Submitted to ***Canadian Geotechnical Journal***

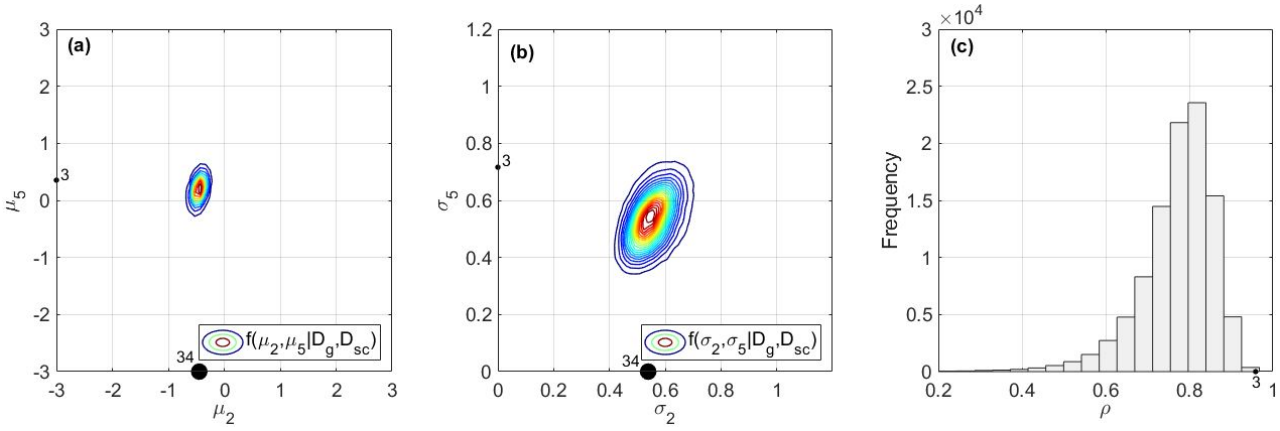

Figure 8 Illustration for (a) $f(\mu_2, \mu_5|D_g,D_{sc})$, (b) $f(\sigma_2, \sigma_5|D_g,D_{sc})$, and (c) $f(\rho|D_g,D_{sc})$.

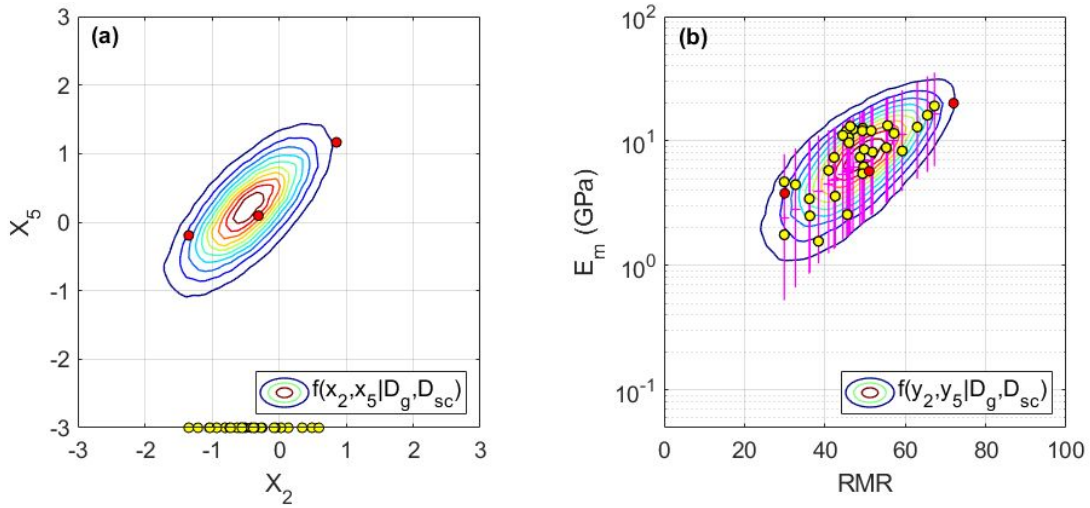

Figure 9 Illustration for the inference stage of HBM: (a) $f(x_2, x_5|D_g, D_{sc})$; (b) inference results.

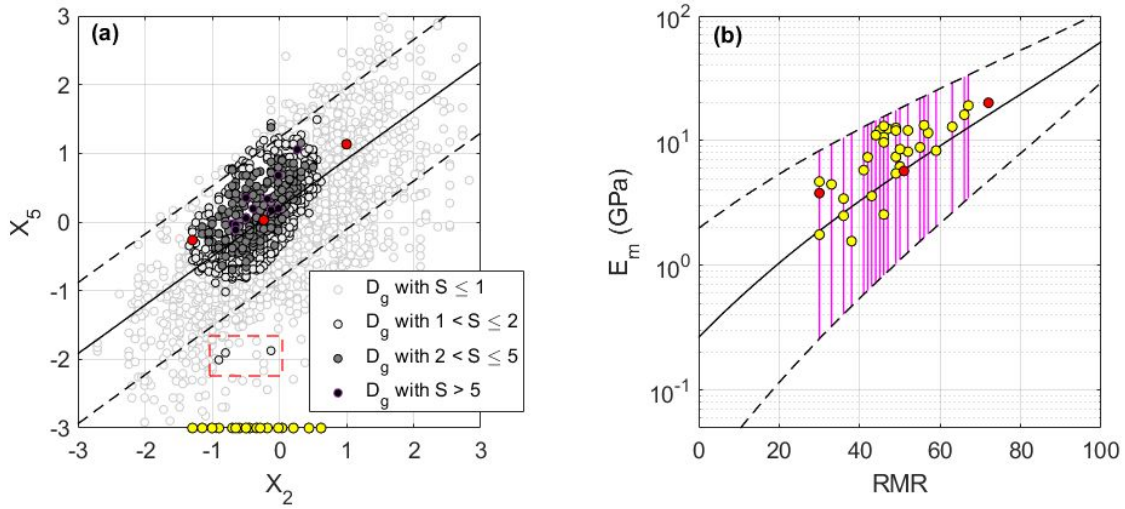

Figure 10 Illustration for SIM: (a) S values; (b) inference results.

Submitted to ***Canadian Geotechnical Journal***

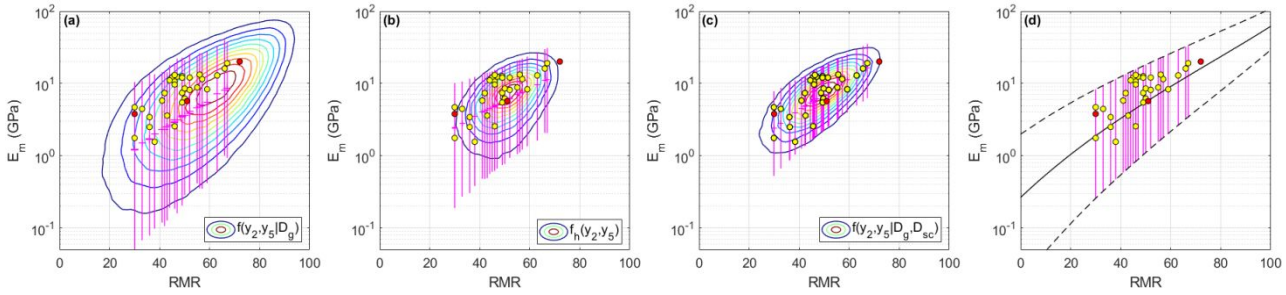

Figure 11 (a-d) Inference results for PMR, HYB, HBM, andSIM for n_{test} = 3.

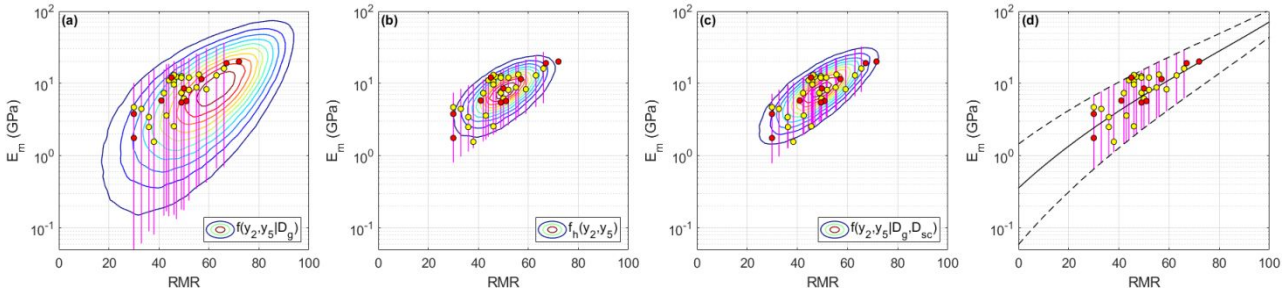

Figure 12 (a-d) inference results for PMR, HYB, HBM, and SIM for n_{test} = 10.

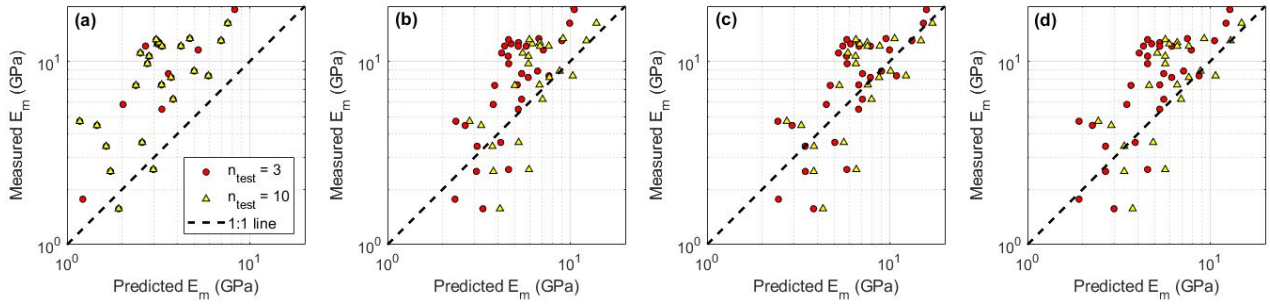

Figure 13 Comparison between the median estimates and measured E_m values: (a) PMR; (b) HYB; (c) HBM; and (d) SIM.

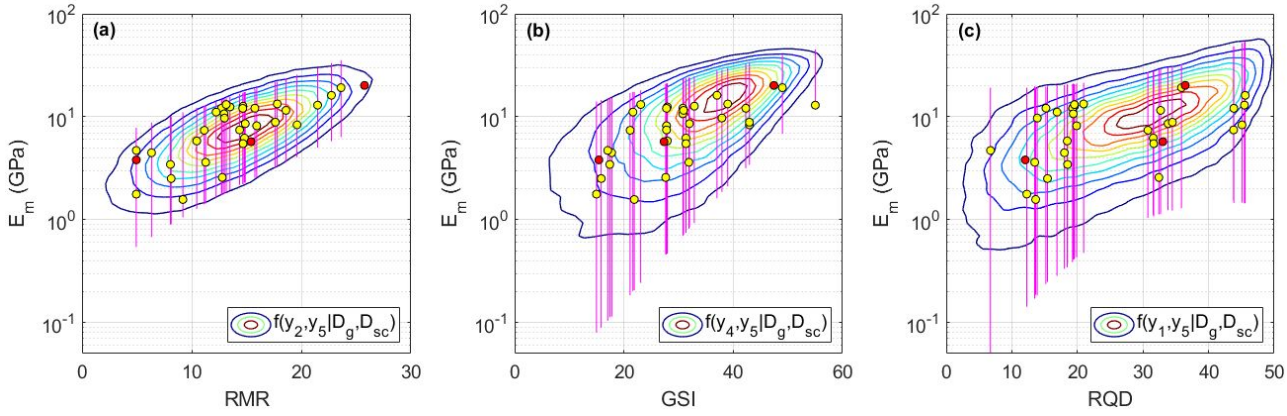

Figure 14 Inference results for HBM if the input variable is (a) RMR, (b) GSI, or (c) RQD.

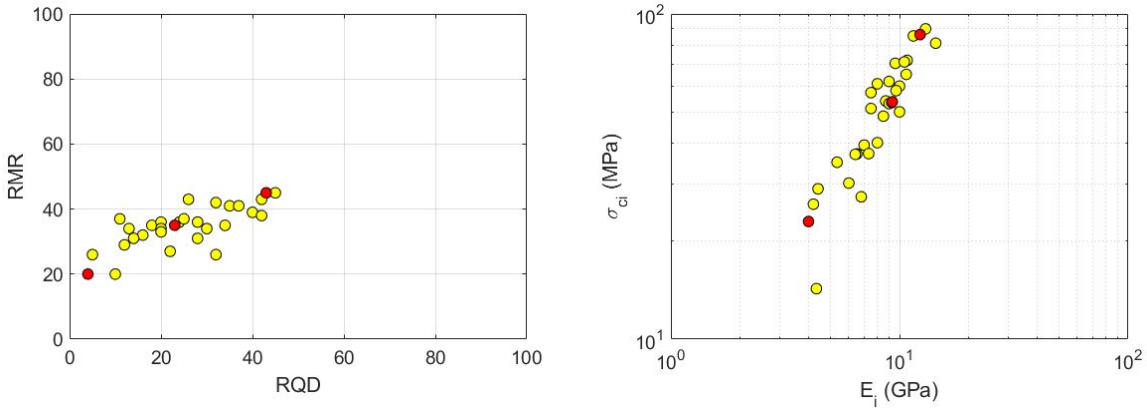

Figure 15 Distribution of D_s cases in Table 8 (red circles are the 10th, 16th, and 22nd cases in the table).

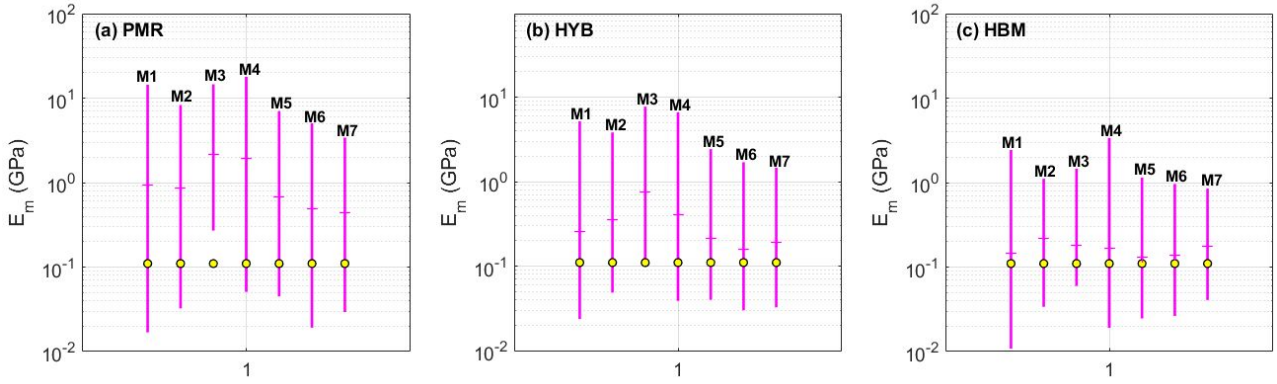

Figure 16 Inference results for Case No. 1 in Table 8: (a) PMR; (b) HYB; (c) HBM.

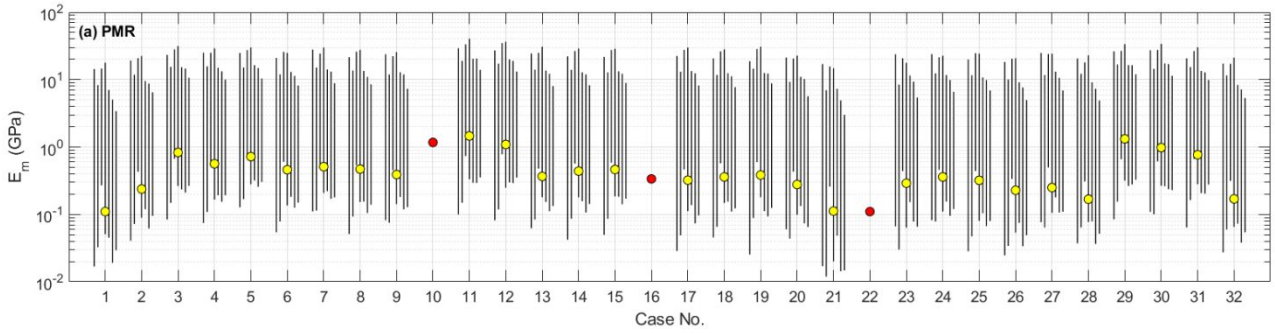

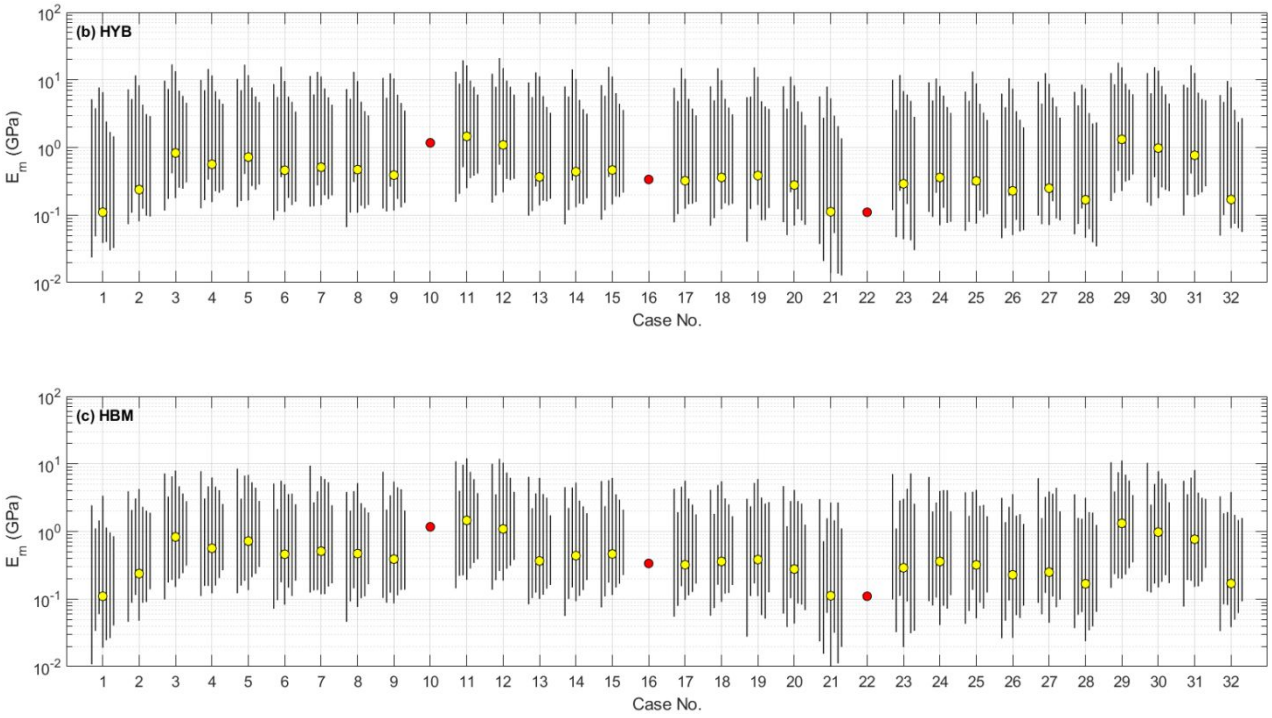

Figure 17 Inference results for (a) PMR, (b) HYB, and (c) HBM.